Journal of Medicinal Chemistry

Drug Annotation

Discovery of Tyrosine Kinase 2 (TYK2) Inhibitor (PF-06826647) for the Treatment of Autoimmune Diseases

Brian S Gerstenberger, Catherine M. Ambler, Eric P Arnold, Mary Ellen Banker, Matthew F. Brown, James D Clark, Alpay Dermenci, Martin E. Dowty, Andrew Fensome, Susan Fish, Matthew M. Hayward, Martin Hegen, Brett D Holingshead, John D. Knafels, David W Lin, Tsung H. Lin, Dafydd R Owen, Eddine Saiah, Raman Sharma, Felix F. Vajdos, Li Xing, Xiaojing Helen Yang, Xin Yang, and Stephen W Wright

J. Med. Chem., **Just Accepted Manuscript** • DOI: 10.1021/acs.jmedchem.0c00948 • Publication Date (Web): 05 Aug 2020

Just Accepted

is published by the American Chemical Society. 1155 Sixteenth Street N.W., Washington, DC 20036

Discovery of Tyrosine Kinase 2 (TYK2) Inhibitor (PF-06826647) for the Treatment of Autoimmune Diseases

Brian S. Gerstenberger,* Catherine Ambler, Eric P. Arnold, Mary-Ellen Banker, Matthew F. Brown, James D. Clark, Alpay Dermenci, Martin E. Dowty, Andrew Fensome, Susan Fish, Matthew M. Hayward, Martin Hegen, Brett D. Hollingshead, John D. Knafels, David W. Lin, Tsung H. Lin, Dafydd R. Owen, Eddine Saiah, Raman Sharma, Felix F. Vajdos, Li Xing, Xiaojing Yang, Xin Yang, and Stephen W. Wright*

Abstract:

Tyrosine kinase 2 (TYK2) is a member of the JAK kinase family that regulates signal transduction downstream of receptors for the IL-23/IL-12 pathways and Type I interferon family, where it pairs with JAK2 or JAK1, respectively. Based on human genetic and emerging clinical data, a selective TYK2 inhibitor provides an opportunity to treat autoimmune diseases delivering a potentially differentiated clinical profile compared to currently approved JAK inhibitors. The discovery of an ATP-competitive pyrazolopyrazinyl series of TYK2 inhibitors was accomplished through computational and structurally-enabled design starting from a known kinase hinge binding motif. By understanding PK/PD relationships, a target profile balancing TYK2 potency and selectivity over off-target JAK2 was established. Lead optimization involved modulating potency, selectivity, and ADME properties which led to the identification of the clinical candidate PF-06826647 (**22**).

Introduction:

Intercellular cytokine signaling plays a critical role in immunological regulation and host immune response in health and disease. Excessive cytokine signaling is a significant contributor to the pathogenesis of autoimmune diseases. Targeting cytokine signaling pathways through pharmacological inhibition or modulation has been shown to be a successful strategy for treatment of several autoimmune and inflammatory diseases.[1] Effective targeting of cytokine signaling pathways via inhibition of Janus kinases (JAK) has been demonstrated as clinically useful in rheumatoid arthritis (RA), psoriatic arthritis, and ulcerative colitis as well as for myeloproliferative disorders and graft-versus-host disease (GvHD).[2, 3] Tyrosine kinase 2 (TYK2) is

one of the four members of the JAK non-receptor tyrosine kinase family which also includes JAK1, JAK2, and JAK3. The JAK kinases are important in both the innate and adaptive immune systems through the modulation of cytokine signaling and their influence on the Signal Transducer and Activation of Transcription (STAT) pathways.[4, 5] TYK2 is associated with the receptors for interleukin-12 (IL-12), IL-23 and type I interferons (IFNs) and regulates the downstream signal transduction pathways.[6,7] These cytokines are critical for the functions of T helper 1 (TH1), TH17, B cells, and myeloid cells that play a key role in a number of autoimmune and chronic inflammatory diseases. JAK kinases function as pairs of homo- or heterodimers in the JAK-STAT pathways. TYK2 pairs with JAK1 to mediate multiple cytokine pathways including type I IFNs, IL-10 and IL-22. TYK2 also pairs with JAK2 to transmit the signals of IL-12 and IL-23.

Genome-wide association studies have identified the TYK2 loci associated with several autoimmune diseases including rheumatoid arthritis, psoriasis, systemic lupus erythematosus, Crohn's disease and ulcerative colitis.[7] A *TYK2* variant encoding a proline to alanine substitution at amino acid 1104 is expressed but is inactive and has been shown to provide protection from several autoimmune diseases.[7, 8] This coding variant has diminished IL-12, IL-23 and type I interferon (IFN) signaling, suggesting that function of TYK2 is critical to the pathogenesis of above mentioned autoimmune diseases. Notably, humans homozygous for this inactive variant do not have an increase in malignancy, bacterial, mycobacterial, fungal or viral infections suggesting that inhibition should be tolerated. Targeting inhibition of IL-12 and IL-23 signaling has been demonstrated in the clinic by ustekinumab (STELARA®), a monoclonal antibody against the p40 subunit common to IL-23 and IL-12, which is approved for the treatment of psoriasis (PsO), psoriatic arthritis, Crohn's disease and ulcerative colitis.[9-11] Additionally, antibodies targeting the IL-23-specific p19 subunit guselkumub (TREMFYA®), tidrakizumab (ILUMYA®) and risankizumab (SKYRIZI®) have been approved for the treatment of adults with moderate to severe plaque psoriasis.[12, 13] The pharmacological profile of a small molecule selective TYK2 kinase inhibitor provides an opportunity to treat several autoimmune diseases with an oral therapy.[14-16]

Currently there are four oral FDA approved JAK kinase inhibitors, tofacitinib (XELJANZ®) (**1**), baricitinib (OLUMIANT®) (**2**), ruxolitinib (JAKAFI®) (**3**), and upadacitinib (RINVOQ®) (**4**) along

with peficitinib (SMYRAF®) (**5**) approved in Japan.[17] All approved JAK kinase inhibitors demonstrate activity against JAK1 without high specificity for TYK2.[18] These compounds bind to the ATP site of the catalytically active Janus Homology 1 (JH1) domain. BMS-986165 (**6**)[19, 20] is a TYK2 inhibitor in phase 3 clinical trials for psoriasis that, in contrast to most other JAK inhibitors, binds to the pseudokinase Janus Homology 2 regulatory domain (JH2). We have previously disclosed the discovery of a JH1 TYK2/JAK1 dual inhibitor brepocitinib (PF-06700841) (**7**) which is currently under clinical investigation for a number of autoimmune indications.[21, 22]

Figure 1: Approved JAK kinase inhibitors and disclosed clinical stage TYK2 kinase inhibitors

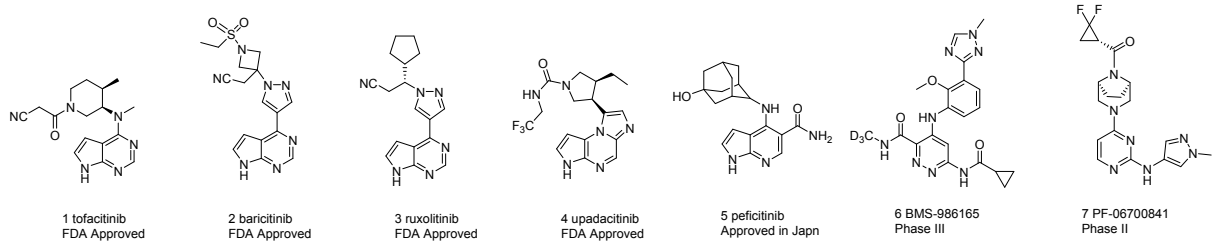

An inhibitor of TYK2 with enhanced selectivity over JAK1, JAK2, and JAK3 could be beneficial based on an orthogonal cytokine inhibition profile driving IL-23, IL-12 and IFNα signaling, while simultaneously sparing suppression of other JAK-dependent cytokines, thus potentially avoiding broader immunosuppression. Sufficient selectivity over JAK2 would be desirable to minimize inhibition of erythropoietin (EPO) and thrombopoietin (TPO) signaling, which is mediated via a JAK2 homodimer. Decreased inhibition of EPO and TPO signaling should minimize effects on the production of red blood cells and platelets that may contribute to anemia and thrombocytopenia seen with some JAK inhibitors.[23] In addition, selectivity over JAK1 and JAK3 would limit inhibition of IL-6 and common gamma-chain family cytokines, including anti-inflammatory cytokines IL-2, IL-15, and IL-21. The overall profile of a TYK2 inhibitor, particularly with clear selectivity over JAK1, is hypothesized to offer the potential for differentiation over the currently approved JAK family-based therapies, while blocking numerous proinflammatory pathways implicated in psoriasis, inflammatory bowel disease (IBD) and other autoimmune diseases.

This manuscript describes the discovery and pre-clinical profile of PF-06826647 (**22**), a potent TYK2 inhibitor binding to the JH1 domain, that is under clinical development for the treatment of psoriasis (PsO), ulcerative colitis (UC), and hidradenitis suppurativa (HS).[24,25,26]

Program Objectives:

The objectives for our TYK2 inhibitor program were based on the clinical and preclinical PK:PD relationships previously observed and discussed for tofacitinib (**1**). Biochemical kinase

assays for TYK2, JAK1, JAK2, and JAK3 and human whole blood cytokine assays, to measure pathway inhibition, were utilized as the primary screens for the SAR campaign. Previous analysis supports that efficacy would be driven by average (C_{av}) IC_{80} coverage of IL-12 as the primary cytokine target of combined TYK2 and JAK2 inhibition.[21, 27] Similar coverage analysis for JAK inhibitors approved for the treatment of RA has been reported. JAK inhibitors for the treatment of RA demonstrate similar profiles of in vitro cytokine receptor inhibition.[28] These drugs inhibit JAK1 with limited selectivity against other JAK family members and show about IC_{80} coverage of IFNα signaling (mediated by JAK1 and TYK2). JAK2-mediated EPO inhibition ($CD34^+$ cells spiked into human whole blood) would be limited to $C_{av} \leq IC_{30}$ to minimize anemia and thrombocytopenia. To enable the analog advancement, a predicted human PK model would be established to calculate target cytokine inhibition levels. For the expedience of regular SAR interpretation, a calculated C_{av} inhibition or IC_{xx}* was used (IC_{xx}* = 100*((IC_{80} IL-12)/ (IC_{80} IL-12 + IC_{50} EPO) to assess functional selectivity.

Results and Discussion

Identification of a selective ATP site inhibitor of TYK2 is challenging due to the high homology across the four JAK isoforms.[29] Rational design of a TYK2 inhibitor requires a hinge binding motif that allows for the optimal scaffolding of vectors to further drive potency and selectivity. In examining the JH1 ATP site of the four JAK kinases, there is a common methionine gatekeeper, however the back pocket is defined by Ile960 in TYK2 which is a valine in the other three JAK family members. This unique amino-acid difference sets the stage for an opportunity to rationally design the hinge group moiety. Overlaying of the pyrrolopyridimidine hinge binding group used in **1**, **2** and **3** shows a 2-point hydrogen bond donor and acceptor interaction with Glu979 and Val981 amino acids (Figure 2A). This binding mode places a steric clash against the larger sidechain of Ile960 in TYK2 and forces the rotation of the lipophilic side chain towards the polar NH of the pyrrolopyridimidine hinge. This can, in part, rationalize why compounds **1**, **2**, and **3** have ~30x, 20x, and 5x decreased potency for TYK2 compared to JAK1, respectively.

Identification of a hinge binding group that does not interact with the carbonyl of Glu969 could resolve the clash with TYK2 Ile960. A [5,6]-fused ring hinge binder with a hydrogen bond

acceptor and donor both to Val981 was proposed to allow for improved TYK2 potency. A [5,6]-fused aromatic system would provide 1) a position off the six-membered ring to build into the P-loop region and 2) a second opportunity to building towards the solvent front to manipulate compound physicochemical properties (Figure 2B). The combination of the steric bulk of the solvent exposed group and the unsubstituted 5-membered ring would prevent the hinge group from flipping the binding mode to use the Glu979 and NH-Val981 positions. Targeting of the Tyr980 and Val981 hinge binding mode was previously exploited in identifying TYK2 active compounds, a strategy which ultimately led to the identification of the TYK2/JAK1 dual inhibitor **7**.

Figure 2: a) Two different TYK2 hinge binding modes: modeled **2** (yellow) superimposed with **7** TYK2 protein X-ray structures (Green, PDB:6DBM) with Ile960 highlighted in purple; b) General scaffolding strategy for a [5,6]-fused ring hinge binder.

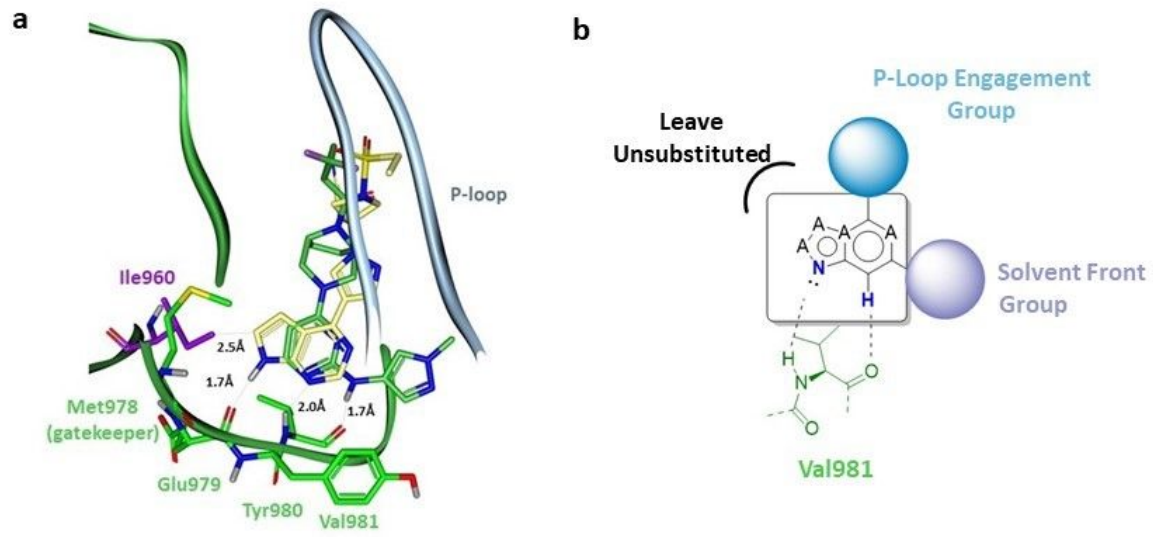

A [5,6]-fused aromatic hinge binding group would require a hydrogen bond acceptor nitrogen atom on the five-membered ring, along with a hydrogen bond donor to project from the 6-membered ring as an aryl C-H (Figure 2B). Analysis and selection of known kinase hinge binding scaffolds as a starting point was used.[30] Polarization of the aryl C-H to increase the hydrogen bonding potential was believed to be necessary to bring about sufficient TYK2 activity and two point binding. To that end several [5,6]-fused aromatic systems were designed and synthesized based off previously known hinge motifs. Initial SAR employed a methylpyrazole moiety as a solvent front group in a similar manner to that used in PF-06700841 (**7**). A substituted trifluoroethylazetidinyl pyrazole group similar to baricitinib to engage the P-loop region was also used. The imidazopyridine **8** was found to have modest potency against TYK2 (enzyme IC_{50} 290 nM) and showed low electrostatic potential on the C-H, which was utilized as a relative measure of H-bond donor ability (Figure 3, Table 1).[31] Addition of a nitrogen into either position of the five-membered ring was calculated to modestly increase the electrostatic C-H potential and thus both the [1,2,4]triazole[1,5]pyridine **9** and [1,2,4]triazole[4,3]pyridine **10** analogs were synthesized. However, compound **9** was found to be only a moderate TYK2 inhibitor (476 nM)

and compound **10** was inactive against TYK2 with an IC_{50} >10 uM. In both cases there was increased electro-positive potential (~ 50 kJ/mol) not only on the C7-H but also on the 2- or 3-positions of the 5-membered ring. These positions face towards the lipophilic gatekeeper the added polarity in this region likely contributed to the reduced TYK2 potency. In addition, the 2-position nitrogen of **10** could also be clashing with the carbonyl oxygen of Glu979 leading to complete loss of TYK2 activity.

With these results in hand, we turned to modification of the six-membered ring system to improve potency. A pyrazole[1,5]pyrazine core[32-38] was of particular interest due to the calculated increased polarization of the C-H for hydrogen bond donor properties (122 kJ/mol). In contrast to **9** and **10**, the most electronegative nitrogen atom was now placed towards the solvent front where it could be better accommodated by bulk water and not clash with the protein (Figure 3). Gratifyingly the pyrazole[1,5]pyrazine analog **11** was found to be a potent TYK2 enzyme inhibitor at 10 nM with a lipophilic efficiency (LipE) of 5.5. With the identification of an appropriately potent and efficient hinge binding core, compound **11** was chosen for further optimization to improve physicochemical properties and JAK selectivity.

Figure 3: [5,6] Fused aromatic TYK2 lead structures **8-11** with electrostatic potential maps calculated in Spartan '18 with Hartree-Fock 6-31G*

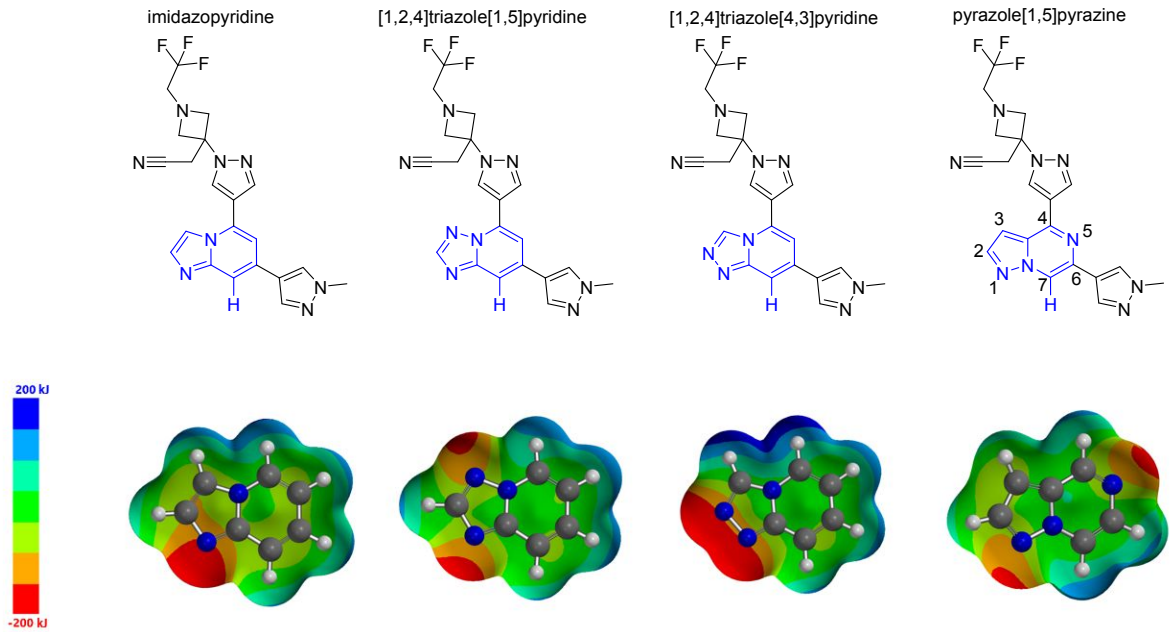

Table 1: TYK2 biochemical IC_{50}, sfLogD, and TYK2 LipE of compounds [5,6] Fused aromatic TYK2 lead structures **8-11**.

Compound #	**8**	**9**	**10**	**11**
TYK2[a] IC_{50} (nM)	290	476	>10,000	10
sfLogD[b]	2.1	2.3	1.2	2.5
TYK2 LipE[c]	4.5	4.0	<3.8	5.5

[a]Enzyme assay. Compounds were assayed at least twice, and the IC_{50} reported as the geometric mean. ATP concentration = 1 mM. [b]Shake-flask LogD (sfLogD) measured between octanol/water phosphate buffered to pH 7.4. [c]LipE = pIC_{50} – LogD;

An X-ray crystal structure of **11** bound to TYK2 confirmed the expected binding mode with N1 accepting a hydrogen bond from the amide NH of Val981 in the TYK2 hinge region (Figure 4a). The proposed polarized C7-H was observed to be 2.4 Å from the carbonyl of Val981, within van der Waals radii. The positioning of the alkyl cyano group was shown to be towards the C-terminal lobe in the active site's lower lipophilic pocket. This mimicked the positioning of the 4*R*-methylpiperidine positioning observed with tofacitinib.[39] The trifluoromethyl azetidine group provided the desired TYK2 kinase potency through engagement of the P-loop, but the moderate LipE of 5.5 reflected the high overall lipophilicity of the molecule. Based on the physicochemical properties and high permeability (MDCK-LE = 18 $x10^{-6}$ cm/sec) the primary clearance mechanism was predicted to be oxidative metabolism.[40] Optimization of the azetidine substituent was guided by LipE through increasing potency/lowering LogD as well as driving towards improving the modest metabolic stability profile of **11** as judged by human liver microsome turnover (HLM) of 18 μL/min/mg protein. In addition, replacement of the trifluoroethyl amino group was preferred due to association with testicular toxicity liability for potential metabolites.[41] The des-fluoro ethyl compound **12** lost approximately 5-fold in TYK2 potency relative to **11** with no change to the overall JAK selectivity profile (Table 2). Interestingly, both compounds showed moderate

metabolic profiles (HLM = 18 and 21 μL/min/mg protein). Attempts to recapitulate the trifluoro-group impact using a cyclopropane analog **13** did not improve potency (TYK2 IC_{50} = 40 nM) and was reflected in a loss of LipE (4.8) and increased HLM clearance (30 μL/min/mg protein).

Figure 4: a) Protein X-Ray structure of **11** bound to TYK2 (Green, PDB: 6X8F) at 2.15 Å with crystallographic waters; b) Overlay of P-loop region of protein X-Ray structure of **11** bound to TYK2 (green) at 2.15Å with Connolly surface and JAK2 (Blue, PDB: 6X8E,) at 1.75Å.

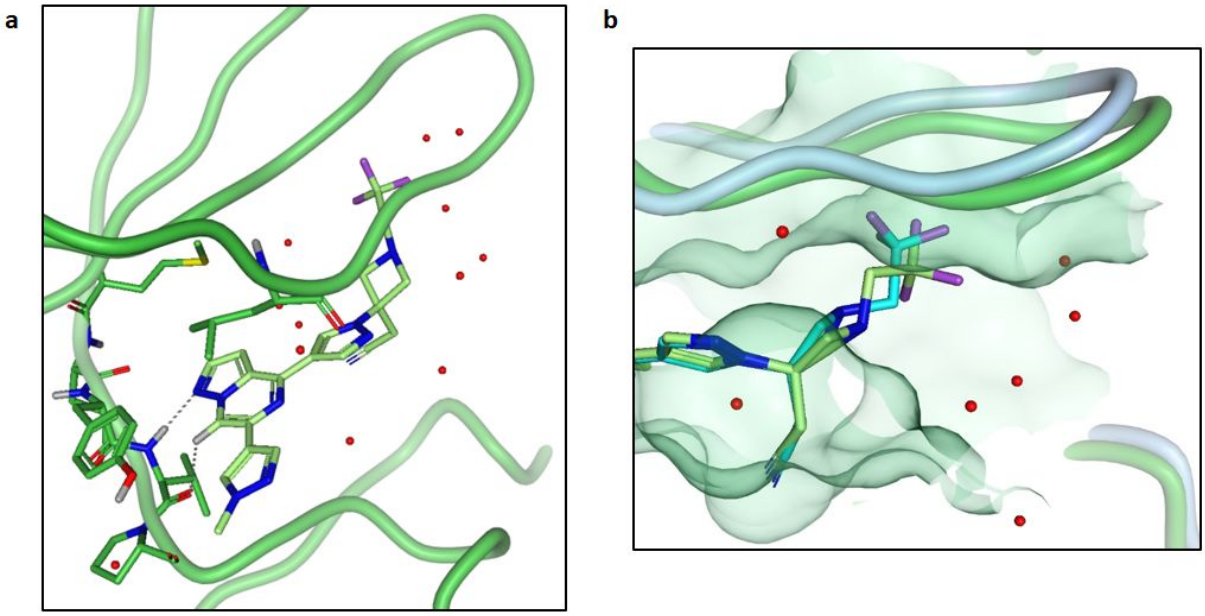

Further attempts to introduce polarity to lower clearance while retaining TYK2 potency provided by the trifluoro group provided mixed results. Introduction of the azetidine amide in compound **14** lowered both sfLogD and brought HLM clearance (< 8 μL/min/mg protein) into the desired range, but also caused a significant loss in potency. This could be due to the amide sp^2 character causing flattening of the azetidine which may not allow the acetyl group to directly engage the P-loop. Appending a hydroxyl to the ethyl group provided compound **15** again showed a loss of potency, even with the increased flexibility of the azetidine N-substituent. In contrast to alkyl groups, **14** and **15** that bear polar groups both had lower permeability as judged by flux in an MDCK-LE cell line (4 $x10^{-6}$ cm/sec). Unique within this series, the cyanomethyl group of compound **16** recapitulated the potency of compound **11**, but also lowered HLM clearance (<8 μL/min/mg protein) and increased LipE to 6.7. Compound **16** showed good selectivity against JAK3 and JAK1, but only a modest 5-fold selectivity against JAK2.

Table 2: SAR of substituted azetidines

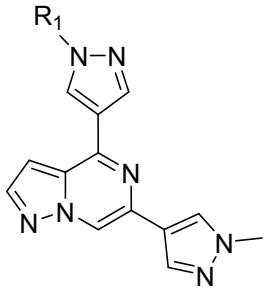

Compound No.	R1	TYK2[a] IC_{50} (nM)	JAK1[a] IC_{50} (nM)	JAK2[a] IC_{50} (nM)	JAK3[a] IC_{50} (nM)	sfLogD[b]	TYK2 LipE[c]	HLM (μL/min/mg protein)	MDCK-LE[42] ($x10^{-6}$ cm/sec)
11	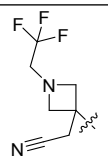	10	358	65	>9,851	2.5	5.50	18	18
12	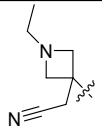	46	2,669	346	>10,000	2.1	5.26	21	33
13	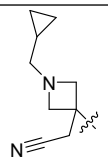	40	933	187	>10,000	2.6	4.84	30	27
14	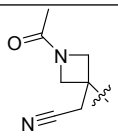	678	6,111	1,747	>10,000	1.2	4.92	<8	4
15	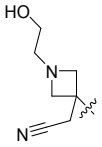	189	5,579	1,044	>10,000	1.2	5.52	<8	7
16	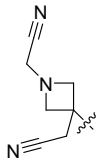	7	250	37	6,682	1.5	6.65	<8	11

[a]Compounds were assayed at least twice, and the IC_{50} reported as the geometric mean. ATP concentration = 1 mM. [b]Shake-flask LogD (sfLogD) measured between octanol/water phosphate buffered to pH 7.4. [c]LipE = pIC_{50} – LogD.

To provide further understanding of JAK2 selectivity, a JAK2 protein X-ray crystal structure of **11** was acquired to compare to the TYK2 structure (Figure 4b). Comparing the protein structures of JAK2 and TYK2 superimposed, the JAK2 P-loop was slightly raised relative to the TYK2 P-loop. Overlay of the two structures and electron density unsurprisingly showed similar binding modes. Subtle interaction differences with the P-loop have been reported to influence selectivity in other JAK inhibitors.[43] The only minor difference seen in the overlay was the azetidine ring configuration. In the JAK2 structure at 1.75 Å resolution, the azetidine adopted a 'trans-like' configuration placing the terminal -CF_3 group towards the P-loop. In contrast, the TYK2 azetidine configuration adopted a 'cis-like' configuration. These observations from the X-ray structures provided the hypothesis that fixing the four-membered ring configuration that could provide the C2-symetric achiral *cis* or *trans* conformations could improve selectivity and replacing the azetidine with a cyclobutane may accomplish this goal.

The methoxycyclobutane diastereomers *cis*-**17** and *trans*-**18** were prepared and both retained TYK2 potency (16 and 22 nM) while the cyclobutane stereoisomer *trans*-**18** showed superior selectivity against JAK1 (68-fold) and JAK2 (10-fold). As expected with the replacement of the azetidine, the methoxycyclobutane analogs showed increased sfLogD and the *cis*-**17** had high clearance as judged by HLM (27 μL/min/mg protein). Somewhat unexpectedly, the isolipophilic *trans*-**18** had very low HLM clearance (< 8 μL/min/mg protein) when compared to the *cis*-**17**. The two diastereomeric *cis*/*trans* isomers demonstrated a useful divergence in clearance in addition to differences in potency and selectivity.

The *cis*-**19** and *trans*-**20** isomers of 2-cyclobutylacetonitrile were prepared as homologs of azetidine **16**. The *cis-**19*** configuration provided a near identical profile to the azetidine **16** while the *trans*-**20** had a slight loss in potency across all JAK isoforms. The JAK2 selectivity of *cis*-**19** and *trans*-**20** were lower than the methoxy analogs **17** and **18** with higher *in vitro* clearances. To improve JAK2 selectivity by further removal of flexibility in the P-loop engagement, truncation

of the 2-cyclobutylacetonitrile to the cyclobutanecarbonitrile group was proposed. The *cis*-**21** cyclobutanecarbonitrile showed excellent TYK2 potency (6 nM) but lacked selectivity against JAK2 (8 nM). In addition, even with the lower measured sfLogD (1.8), significant clearance was still observed (HLM = 17 μL/min/mg protein), in line with the previous results for *cis*-**17**. In contrast, the *trans*-**22** cyclobutanecarbonitrile (PF-06824467) showed good selectivity against JAK1 and JAK2 with very low HLM clearance (<8 μL/min/mg protein) consistent with *trans*-**20**.

Table 3: Influence of cyclobutane substituent on potency, sfLogD, and metabolism of compounds **17-22**.

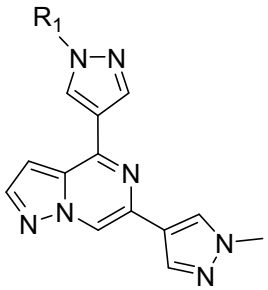

Compound No.	R1	TYK2[a] IC_{50} (nM)	JAK1 [a] IC_{50} (nM)	JAK2 [a] IC_{50} (nM)	JAK3 [a] IC_{50} (nM)	sfLogD[b]	TYK2 LipE[c]	HLM (µL/min/mg protein)	MDCK-LE[42] (x10^{-6} cm/sec)
17	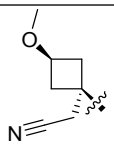	16	664	99	>10,000	2.2	5.65	27	20
18	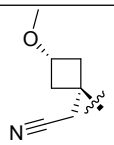	22	1,495	228	>9121	2.3	5.41	<8	22
19	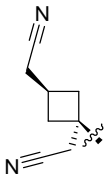	8	273	38	>6,170	1.8	6.32	10	21
20	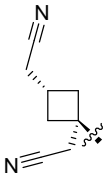	24	764	159	>10,000	1.9	5.74	11	20
21	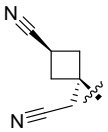	6	21	8	1,051	1.8	6.47	17	15
22	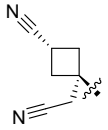	15	383	74	>10,000	1.7	6.09	<8	17

[a]Compounds were assayed at least twice, and the IC_{50} reported as the geometric mean. ATP concentration = 1 mM. [b]Shake-flask LogD (sfLogD) measured between octanol/water phosphate buffered to pH 7.4. [c]LipE = pIC50 – LogD.

To better understand the interactions of the cyclobutane analogs with TYK2, a protein X-ray crystal structure of **22** was acquired. The cis cyclobutanecarbonitrile moiety was positioned below and towards the tip of the P-loop (Figure 5a). Simulated waters in the apo structure showed a calculated high energy water molecule (δG = 5.3 kcal/mol) in this region.[44] The end of the P-loop contains mainly hydrophobic residues and a generally satisfied hydrogen bond network which may contribute to the calculated lability of this modeled water in the apo structure. This predicted high energy water is displaced by the cyclobutanecarbonitrile group of **22**. The electrostatic mapping of this pocket also showed a positive electrostatic potential which could provide a favorable interaction with the cyano group (Figure 5a). The optimized hinge binding group along with the rationally designed interactions with the P-loop combined to give potent TYK2 inhibition.

Figure 5: a) Protein X-ray structure of **22** in TYK2 (Yellow, PDB: 6X8G)) at 2.21Å with electrostatic potential map and modeled APO waters in the P-loop (spheres); b) Top view of the hinge and solvent exposed region of the protein X-ray structure of **22** showing 2-point hinger interaction with Val981

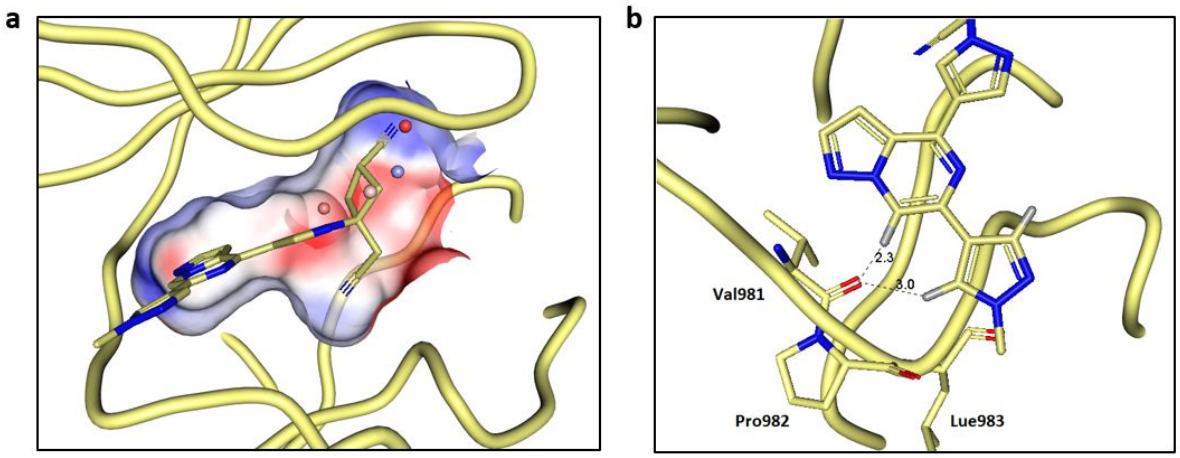

Based on the TYK2 potency, JAK selectivity profile, and low clearance, **22** was selected to further explore the SAR of the pyrazole group (R2) (Table 4). The SAR was also explored on the more potent but less JAK1 selective *trans*-**21** in order to attempt to improve TYK2 selectivity in a parallel effort. A matrix of pyrazole structural analogs were made in an attempt to further tune the properties. The presumed solvent exposed methyl group on the pyrazole was hypothesized to be inefficient lipophilicity (Figure 5b). Removal of the methyl group from the 4-pyrazole in the *cis*-**23** and *trans*-**24** pair showed an increase in HLM clearance despite reduction in LogD and lowered the permeability as measured by MDCK-LE. Neither compound showed improvement from their corresponding methyl analogs with no improvement in JAK1 selectivity from **21** to **23** and an erosion of TYK2 potency from **22** to **24**. In order to improve the permeability of the NH pyrazole, the 1*H*-3-pyrazole would allow a tautomer to place the N-H towards the core nitrogen and mask the H-bond donor via an intermolecular hydrogen bond. This strategy wasn't successful when applied to *cis*-**25**, but gratifyingly, the *trans*-**26** analog showed improved permeability compared to **24**. In addition, TYK2 potency was partially regained while retaining low HLM clearance. Finally, the 1-methyl-3-pyrazole analogs were synthesized. In the case of *cis*-**27** there was a gain in JAK1 and JAK2 selectivity, but this was still a higher clearance compound

based on HLM. *Analog trans*-**28** had weaker TYK2 potency compared to **22** but had similar low clearance and JAK selectivity.

Table 4: SAR of the hinge pyrazole region compounds **23-28.**

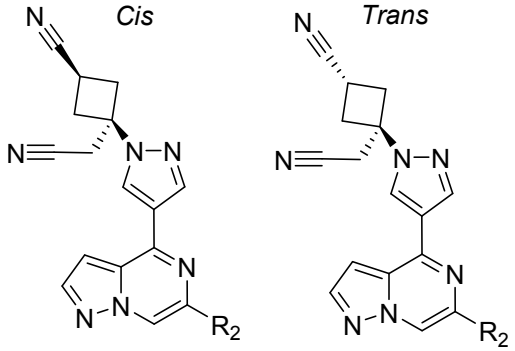

Compound No.	Cyclo-butane Stereo-chemistry	R2	TYK2[a] IC_{50} (nM)	JAK1[a] IC_{50} (nM)	JAK2[a] IC_{50} (nM)	JAK3[a] IC_{50} (nM)	sfLogD[b]	TYK2 LipE[c]	HLM (μL/min/mg protein)	MDCK-LE[42] ($x10^{-6}$ cm/sec)
23	Cis	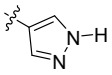	8	22	22	2,242	1.6	6.52	44	6
24	Trans		44	398	280	>10,000	1.7	5.39	19	7
25	Cis	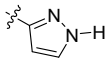	9	43	31	4,448	1.7	6.37	20	7
26	Trans		26	284	172	>10,000	1.7	5.88	<8	17
27	Cis	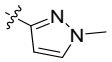	10	261	45	>9,588	1.6	6.40	23	14
28	Trans		67	2,534	467	>10,000	1.6	5.64	<8	20

[a]Compounds were assayed at least twice, and the IC_{50} reported as the geometric mean. ATP concentration = 1 mM. [b]Shake-flask LogD (sfLogD) measured between octanol/water phosphate buffered to pH 7.4. [c]LipE = pIC50 – LogD.

A selection of compounds that showed both TYK2 biochemical potency and low *in vitro* metabolic clearance (HLM <8 μL/min/mg protein) were selected to advance into profiling in human whole blood (HWB) cytokine assays. These assays were established to identify the desired candidate profile with respect to efficacy and off-target effects. Inhibition of IL-12-stimulated phosphorylation of STAT4 was selected as the efficacy driver and blockade of EPO-

induced phosphoSTAT5 was the key selectivity measurement. The project objective was to achieve potent IL-12 inhibition (IC_{50} < 50 nM) with a selectivity profile of IC_{xx} < 0.30 on EPO when set to a calculated IC_{80} of IL-12 coverage. For all compounds, human plasma protein binding was measured to correct for free-drug potency. The compounds profiled were moderately bound with fraction unbound ranging from 0.2 - 0.5 (Table 5). In addition, *in vitro* clearance was further profiled using human hepatocytes (HHEP) as a complement to the HLM data (CYP450 metabolism) in order to cover both phase I and II metabolic processes.

Of the compounds selected for this more extensive profiling, methoxycyclobutane **18** [PF-06799018] showed the largest TYK2/JAK2 selectivity at 10-fold. Unfortunately, even with good TYK2 biochemical potency (22 nM) there was only moderate inhibition in HWB of IL-12 ($IC_{50,u}$ 186 nM). Compound **18** had a low metabolic clearance (HHEP = 6 μL/min/mil cells). Both **26** and **28** had weaker TYK2 potency and more moderate JAK2 selectivity which translated into weak overall IL-12 inhibition ($IC_{50,u}$ 334 and 254 nM respectfully). Compound **21** was the most potent compound identified on TYK2 which drove strong potency against IL-12 ($IC_{50,u}$ 9 nM). However insufficient biochemical selectivity against JAK2 meant there was an unacceptably high coverage of EPO (IC_{63}). In addition, **21** showed a moderate but increased clearance profile (HHEP =12 μL/min/mil cells). The *cis*-cyclobutane **22** showed weaker TYK2 enzyme activity compared to its stereoisomer **21**, but with more selectivity against JAK2. With this profile, **22** provided the desired level of IL-12 potency ($IC_{50,u}$ 14 nM). Compound **22** also demonstrated the desired selectivity profile with an IC_{28} for EPO coverage at the IL-12 IC_{80}, and a very low in vitro clearance profile (HHEP <3 μL/min/mil cells). Further profiling of **22** against a panel of 231 kinases at non-physiologically conditions for each kinase Km showed 21 non JAK kinases with >50% at 1 uM dose. However, a kinase biochemical promiscuity panel against 40 kinase targets at physiologically relevant conditions with the 1 mM ATP and under those conditions no kinase target screened in both formats had >50% inhibition. (ThermoFisher Kinase Profiling, See Supplementary Table 1)[45] Based on the strong IL-12 potency, acceptable off-target profile, and excellent metabolic clearance profile, **22** was selected to advance to *in vivo* profiling.

Table 5: HWB cytokine and HHEP profile of potent TYK2 compounds **18**, **21**, **22**, **26**, and **28**.

Compound No.	Human Plasma Protein Binding F_u[a]	TYK2 IC_{50} nM (TYK2/JAK2 approx. fold selectivity)	IL-12 Free IC_{50} (nM)[b]	EPO Free IC_{50} (nM)[b]	ICxx EPO[c]	HHEP (µl/min/mil cells)
18	0.30	22 (10x)	186	1,100	0.41	6
21	0.34	6 (1x)	9	22	0.63	12
22	0.38	15 (5x)	14[e]	148[e]	0.28	< 3
26	0.32	26, (7x)	334	*nd*[d]	*nd*[d]	7
28	0.20	67 (7x)	254	*nd*[d]	*nd*[d]	< 2

[a]Fraction unbound in human plasma. [b]Compounds were assayed at least twice, and the IC_{50} reported as the geometric mean, Free IC_{50} calculated using assumed blood to plasma concentration ratio = 1. [c]ICxx EPO = 1 / ((EPO IC_{50}/(4 x IL-12 IC_{50})+1). [d]Not determined. [e]Free IC_{50} calculated by whole blood IC50 * Fu / measured blood to plasma concentration ratio.

The physical properties of **22** include a basic pK_a of <1.7 indicating the compound would be neutral at physiological pH. The measured logD at pH 7.4 was 1.7. Thermodynamic solubility of the crystalline material was low at 0.8 µM (0.3 µg/mL) at pH 7.4, and a salt formation strategy to improve solubility could not be pursued due to the lack of ionizable groups. A Spray Dried Dispersion (SDD) formulation improved experimental intestinal solubility to approximately 160-180 µM (60-70 µg/mL). Compound **22** showed high passive permeability in MDCK-LE cells (mean Papp 16.7 x 10^{-6} cm/s) but is a substrate for MDR1 (efflux ratio >6) and BCRP (efflux ratio >2) efflux transport.[46]

The pharmacokinetics of **22** were studied in Sprague-Dawley rats. Following a 1 mg/kg intravenous dose, the systemic clearance was 12 mL/min/kg, the steady state volume of distribution (V_{ss}) was 1.1 L/kg, and the AUC_{inf} was 1,380 ng·h/mL. Following oral administration of the crystalline (non-SDD) material at 3 and 30 mg/kg in 0.5% methylcellulose, oral bioavailability was 15 and 8% respectively. Oral bioavailability significantly improved to 58 and

63% at 3 and 30 mg/kg respectively when dosed in a SDD at 25% drug load, indicating an improved fraction absorbed of >75%. At 3 and 30 mg/kg in SDD, the respective C_{max} was 369 and 2,780 ng/mL and the respective AUC_{inf} was 2,390 and 25,900 ng·h/mL. Plasma protein binding was 18% in rat and 38% in human without significant blood to plasma distribution (1.4 in human).

The *in vitro* metabolism of **22** was studied in human liver microsomes (<8 µL/min/mg protein) and hepatocytes (1.8 µL/min/million cells), both of which indicated low metabolic turnover (Table 6). Oxidative metabolites of **22** accounted for the primary routes of biotransformation in rat, monkey, and human *in vitro* hepatic systems consistent with CYP450 metabolism. Primary metabolic pathways included *N*-demethylation of the pyrazole, hydroxylation of the pyrazole, and addition of oxygen and loss of the nitrile groups. Renal (1.3%) and bile (0.9%) excretion was low in the rat. Considering the importance of CYP450 metabolism, human clearance predictions were made using both human liver microsomes and hepatocyte scaling (well-stirred model) indicating a blood clearance of 2.3 and 1.5 mL/min/kg, respectively. The V_{ss} was predicted to be 1.2 L/kg using SimCYP® PBPK modeling, consistent with the neutral properties of the compound. Oral bioavailability was expected to be dose-dependent based on low solubility characteristics and the need for a solubility enabling formulation.

Table 6: Summary of predicted human blood pharmacokinetics of **22** from *in vivo* and *in vitro* systems

Method	Human Prediction	
	CL_b (mL/min/kg)	**V_{ss} (L/kg)**
Human Liver Microsomes	2.3	
Human Relay Hepatocytes	1.5	
Rat Single Species	5.2	2.3
SimCYP® PBPK modeling		1.2

CL_b: blood clearance; V_{ss}: volume of distribution at steady state; PBPK: physiologically based pharmacokinetics: Human clearance predictions from in vitro systems were scaled based on the well-stirred model or single species scaling from allometry[47,48]

The overall cytokine inhibition profile (IC_{XX}) was calculated for **22** based upon the modeled daily C_{av} exposure (i.e. AUC/dosing interval = 56 nM unbound) to cover the calculated IC_{80} of IL-12 (unbound IC_{50} 14 nM x 4 = 56 nM). Relative average daily cytokine inhibition representing different JAK signaling pairs is shown in Table 7 and Figure 6.

Table 7: Human whole blood potencies for **22** with different cytokine stimuli, and IC_{XX} calculated from predicted C_{av} exposure to cover IL-12 IC_{80}.

Human whole blood	JAK Signaling Complex	Uncorrected IC_{50} (nM) Mean ± SD[a]	IC_{xx}[b]
IL-12-induced pSTAT4 IC_{50} (lymphocytes)	TYK2/JAK2	53 ± 16	0.80
IL-23-induced pSTAT3 IC_{50} (lymphocytes)	TYK2/JAK2	112 ± 18	0.65
IFNα-induced pSTAT3 IC_{50} (lymphocytes)	TYK2/JAK1	66 ± 21	0.76
IL-10-induced pSTAT3 IC_{50} (lymphocytes)	TYK2/JAK1	427 ± 157	0.33
IL-27-induced pSTAT3 IC_{50} (lymphocytes)	TYK2/JAK1/JAK2	201 ± 25	0.51
IL-6-induced pSTAT1 IC_{50} ($CD3^+$cells)	TYK2/JAK1/JAK2	566 ± 283	0.27
IL-6-induced pSTAT3 IC_{50} ($CD3^+$ cells)	TYK2/JAK1/JAK2	4,370 ± 1,260	0.05
IL-21-induced pSTAT3 IC_{50} (lymphocytes)	JAK1/JAK3	4,890 ± 2,550	0.04
IL-15-induced pSTAT5 IC_{50} (lymphocytes)	JAK1/JAK3	4,840 ± 2,260	0.04
IL-2-induced pSTAT5 IC_{50} (lymphocytes)	JAK1/JAK3	3,740 ± 270	0.05
IFNγ-induced pSTAT1 IC_{50} ($CD14^+$)	JAK1/JAK2	2,220 ± 750	0.09
EPO-induced pSTAT5 (spiked $CD34^+$ progenitor cells)	JAK2/JAK2	547 ± 195	0.28

[a]Compound **22** was assayed at least three times in each assay, and the IC_{50} reported as the geometric mean. SD = standard deviation. b [c]ICxx cytokine = 1 / ((Whole blood IC_{50}/(4 x IL-12 IC_{50})+1).

Figure 6. Radial plot of cytokine inhibition IC_{xx} relative to the IL-12 IC_{80} for compound **22**, derived from potency in human whole blood assays and predicted average daily human plasma drug concentration.

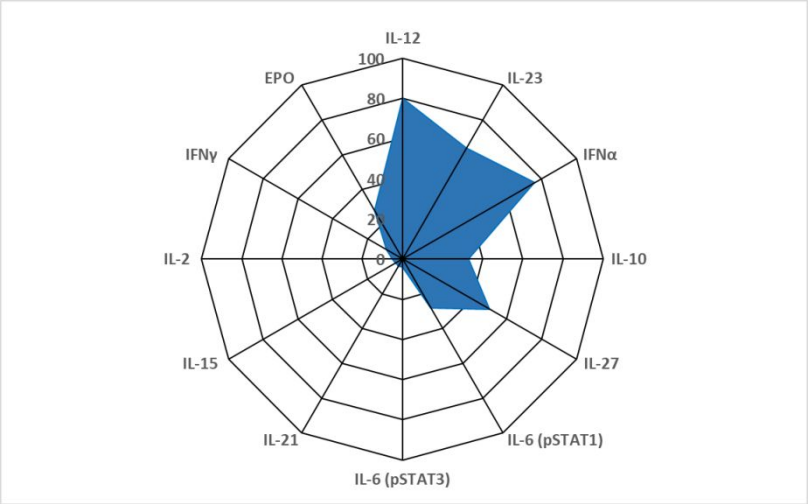

Efficacy of **22** was evaluated in the mouse imiquimod-induced skin inflammation model employing a therapeutic dosing paradigm previous used to profile **1** of an anti-p40 antibody.[49] In this mouse skin inflammation model, the subjects are challenged with topically-applied imiquimod (Toll-Like Receptor 7 and 8 agonist) on the ear to induce inflammation followed by oral dosing of **22**. In this mouse model, the murine TYK2 gene was modified by introducing a humanizing point mutation in order to change amino acid 980 of murine TYK2 protein from valine to isoleucine. This was done in order to compensate for an observed species potency shift driven by this amino acid difference between human and preclinical species.[50] Oral treatment with **22** at 30, 10, and 3 mg/kg, once per day (QD) reduced clinical endpoints associated with skin inflammation in this model. The measured average unbound daily concentrations ($C_{av,u}$ nM) of 1, 3, 10, and 30 mg/kg were 14.5, 45.7, 225, and 668 nM respectively, resulting in average IL12 inhibition of 51, 77, 94, and 98%. No significant effect on ear thickness was seen at 1 mg/kg compared to control animals at the end of the 5-day study.

Figure 7: Compound **22** dosed at 30, 10, 3, and 1 mg/kg, PO, QD inhibited ear swelling in the imiquimod-induced skin inflammation model. Compound **22** significantly inhibited ear swelling when compared to the vehicle-treated mice (n=12) (30 mg/kg, 46.2%, p=0.0004, 10 mg/kg, 34%, p=0.0145, and 3 mg/kg, 31.3% (0.0198). The effect of the 1 mg/kg dose was not statistically significant (ns) when compared to the vehicle-treated mice.

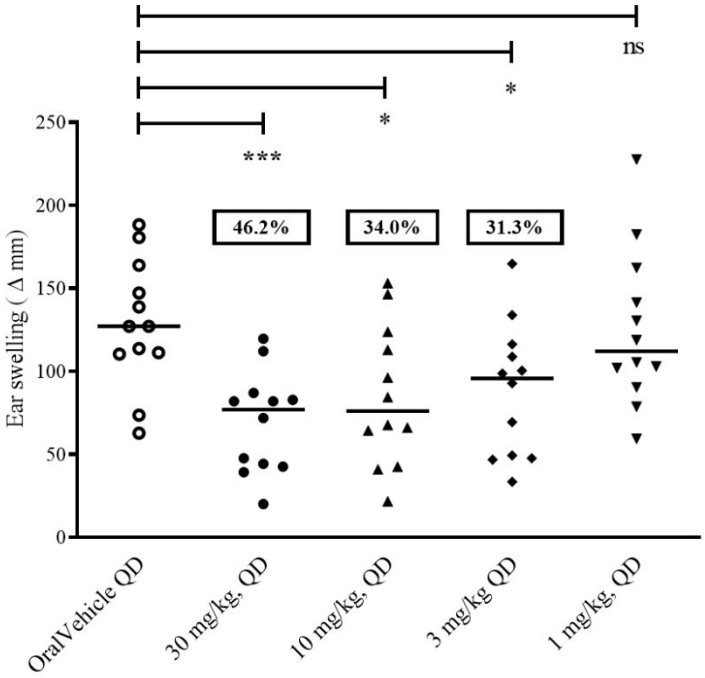

Chemistry

Synthesis of the [5,6]-fused heterocycle structures **8**, **9** and **10** was accomplished as shown in Scheme 1. Conjugate addition of 4-(4,4,5,5-tetramethyl-1,3,2-dioxaborolan-2-yl)-1H-pyrazole (**29**) with *tert*-butyl 3-(cyanomethylene)azetidine-1-carboxylate (**30**)[51] gave the elaborated pyrazole boronate **31**, which underwent Suzuki-Miyaura coupling independently with **32** and **33** to provide **35** and **34**, respectively (see Supporting Information). A second Suzuki-Miyaura coupling of 1-methyl-4-(4,4,5,5-tetramethyl-1,3,2-dioxaborolan-2-yl)-1H-pyrazole with **34** and **35** afforded **36** and **37**, respectively. The syntheses were completed by BOC deprotection and azetidine alkylation with 2,2,2-trifluoroethyl triflate to provide **8** from **36** and **9** from **37**. The alkylation of the deprotected azetidines required neutralization of the acid addition salts

obtained by BOC deprotection and elimination of chloride or trifluoroacetate counterions prior to exposure to 2,2,2-trifluoroethyl triflate. The presence of chloride was found to result in the formation of unreactive 2,2,2-trifluoroethyl chloride, while the presence of trifluoroacetate ion was found to result in the formation of 2,2,2-trifluoroethyl trifluoroacetate, which in turn afforded the azetidine trifluoroacetamides as a serious competing reaction. Similarly, compound **38** (see Supporting Information) underwent Suzuki-Miyaura coupling with (1-(*tert*-butoxycarbonyl)-1H-pyrazol-4-yl)boronic acid to provide **39** after BOC deprotection *in situ*. Conjugate addition of **39** with **30** gave the N-BOC azetidine **40**. BOC deprotection followed by azetidine alkylation with 2,2,2-trifluoroethyl triflate completed the synthesis of **10**.

Scheme 1: Synthesis of **8**, **9**, and **10**

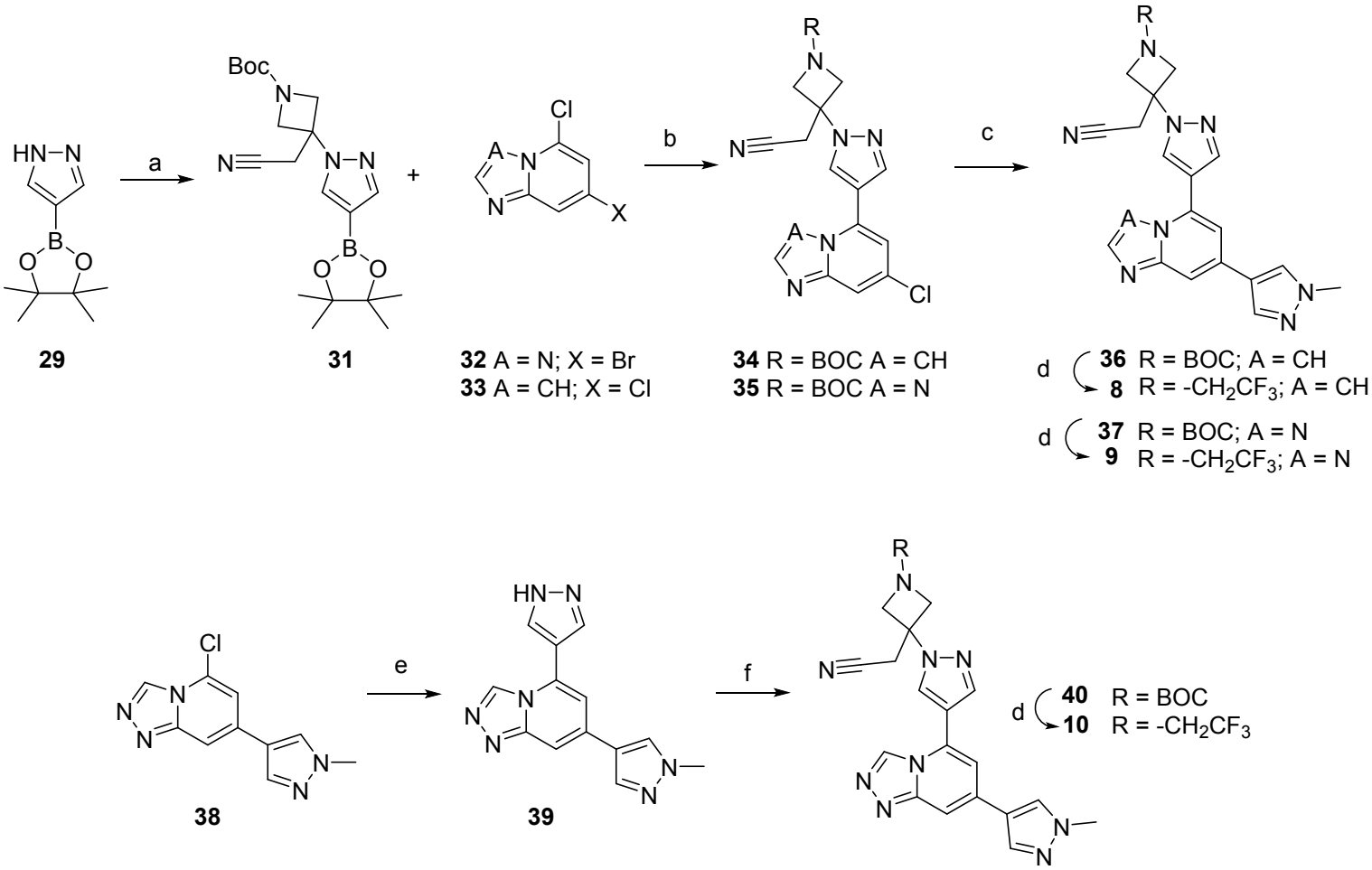

Reagents and conditions: (a) **30**, DBU, MeCN, 50-90 °C, 4-18 h; (b) K_2CO_3 or Cs_2CO_3, Pd(dppf)Cl_2, 1,4-dioxane, H_2O, 95–100 °C, 16 - 48 h; (c) 1-methyl-4-(4,4,5,5-tetramethyl-1,3,2-dioxaborolan-2-yl)-1*H*-pyrazole, K_2CO_3 or CsF, Pd(dppf)Cl_2, 1,4-dioxane or Et(Me)$_2$COH, 70–100 °C, 18 - 48 h; (d) 1. MsOH or HCl, MeCN or dioxane, 20–30 °C, 16–20 h; 2. CF_3CH_2OTf, DIEA, DMF or MeCN, 0–20 °C, 2–24 h. (e) (1-(*tert*-butoxycarbonyl)-1*H*-pyrazol-4-yl)boronic acid, Cs_2CO_3, Pd(dppf)Cl_2, 1,4-dioxane, H_2O, 95 °C, 16 h; (f) **30**, DBU, MeCN, 30 °C, 16 h.

The pyrazolo[1,5-a]pyrazine analogues (**11**–**22**) required a longer synthetic sequence to allow the selective installation of the differentially functionalized pyrazole substituents at the 4- and 6-positions of the pyrazolo[1,5-a]pyrazine ring. Initially, the N-methyl pyrazole at the 6-position was introduced at the beginning of the synthesis so that its placement in the pyrazolo[1,5-a]pyrazine ring system would be unambiguous following construction of the pyrazine ring (Scheme 2). Reaction of the α-bromoketone **41** (see Supporting Information)[52] with diethyl 1H-pyrazole-3,5-dicarboxylate **42** provided **43.** This route was selected to avoid regioselectivity issues associated with attempts to alkylate ethyl pyrazole-3-carboxylate.[53] Ketone **43** was cyclized to the pyrazolo[1,5-a]pyrazine **44** by condensation with ammonium acetate.[54] Saponification to **45** followed by thermal decarboxylation gave the pyrazolo[1,5-a]pyrazin-4(5H)-one **46**, which was treated with phosphoryl chloride to provide the key chloro pyrazolo[1,5-a]pyrazine intermediate **47**.

Scheme 2: Synthesis of **47**

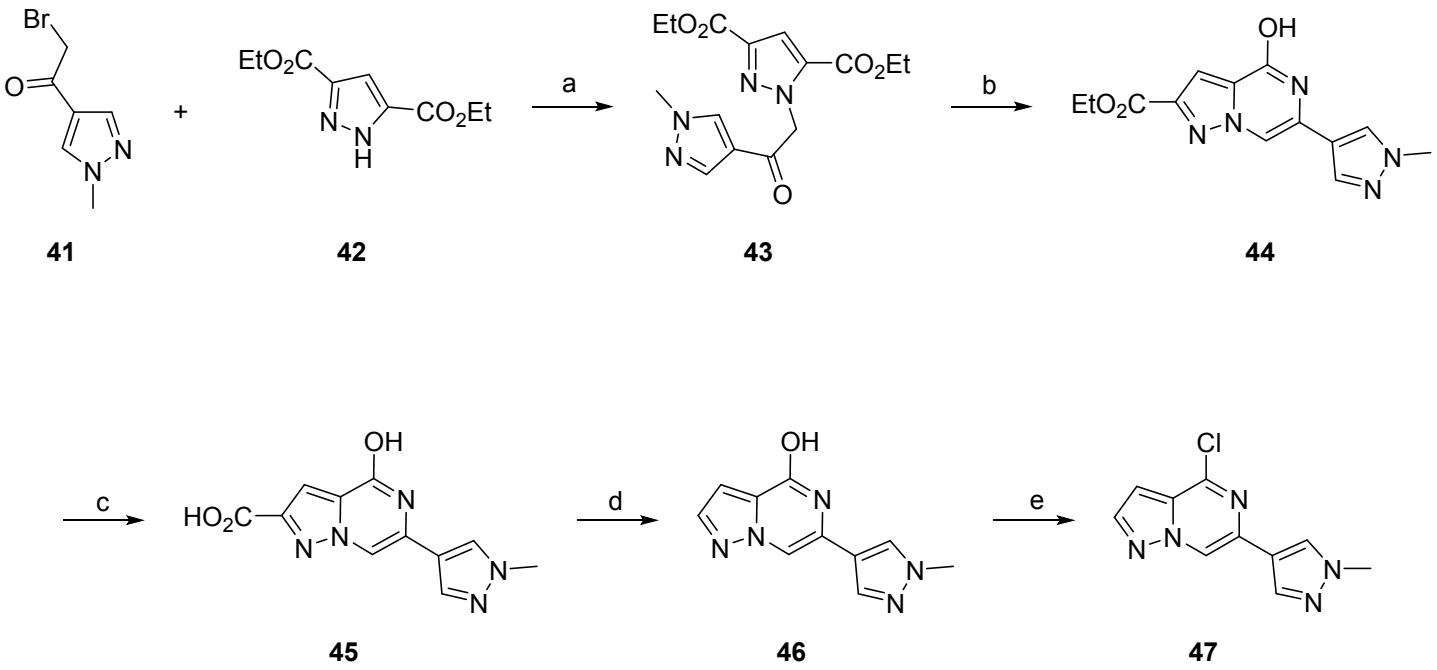

Reagents and conditions: (a) **42**, Cs_2CO_3, DMF, 20 °C, 18 h; (b) NH_4OAc, EtOH, 130 °C, 24 h; (c) NaOH, MeOH, H_2O, 20 °C, 18 h; (d) sulfolane, 280 °C, 2 h; (e) $POCl_3$, MeCN, 85 °C, 48 h.

The compounds **23–28** shown in **Table 4** required the previously unknown 4,6-dichloropyrazolo[1,5-a]pyrazine intermediate **52** (Scheme 3). Alkylation of ethyl pyrazole-3-carboxylate (**48**) with $ClCH_2CN$ yielded predominantly the desired proximal regioisomer **49**. The regiochemical outcome of this alkylation was opposite with the results obtained using α-halo carbonyl electrophiles in similar alkylations. Nitrile hydrolysis with H_2SO_4 in TFA gave the primary amide **50**. Underwent base–mediated cyclization of **50** followed by neutralization with HCl to the pyrazolo[1,5-a]pyrazine-4,6-dione **51,** which was carried forward to chlorination with phosphoryl chloride to provide **52**. Sequential diversification of **52** *via* Suzuki-Miyaura, Stille, and Negishi coupling methodologies could be accomplished under mild conditions with excellent functional group tolerance.

Scheme 3: Synthesis of dichloro pyrazolopyrazine **52**

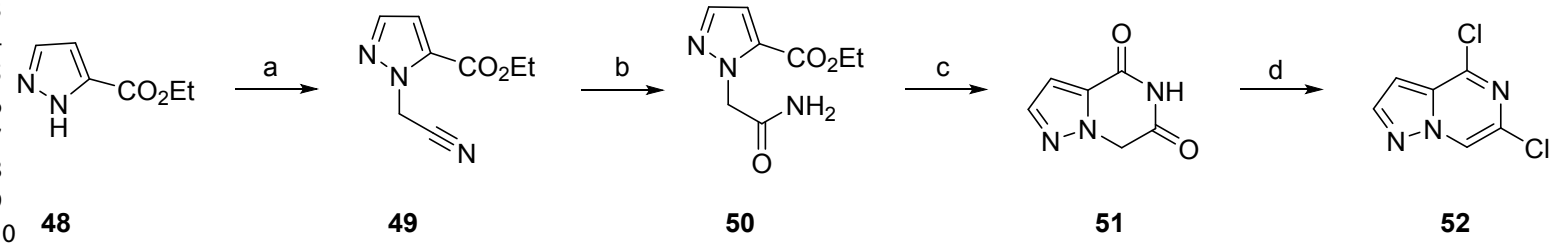

Reagents and conditions: (a) $ClCH_2CN$, Cs_2CO_3, DMF, 25 °C, 16 h; (b) H_2SO_4, TFA, 25 °C, 16 h; (c) NaO*t*-Bu, EtOH, THF, 70 °C, 16 h; (d) $POCl_3$, PyHCl, 120 °C, 18 h.

The syntheses of the necessary cyclobutyl-substituted pyrazole boronates (**59**–**64**) were accomplished as shown in **Scheme 4**. Substituted cyclobutanones **53**–**55** (see Supporting Information) were subjected to Horner–Wadsworth–Emmons reaction with diethyl (cyanomethyl)phosphonate[55] to provide substituted 2-cyclobutylideneacetonitriles **56**–**58**. Conjugate addition of **29** with **56**–**58** in the presence of DBU was followed by separation of the resulting *trans* (**59**–**61**) and *cis* (**62**–**64**) cyclobutane isomers. The conjugate addition reactions of **56**–**58** proceeded with good overall conversion and a generally clean reaction profile. The *trans* or *cis* relationships between the pyrazole ring and the distal cyclobutane substituents (CH_2CN, OCH_3, or CN) was readily be established by nOe experiments.

Scheme 4: Syntheses of *trans* and *cis* cyclobutyl - substituted pyrazole boronates **59** - **64**

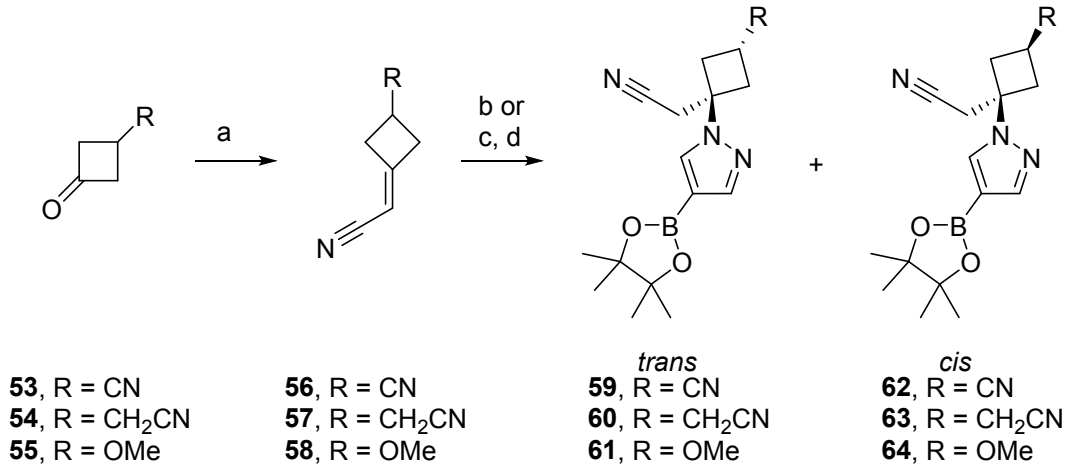

Reagents and conditions: (a) $NCCH_2P(O)(OEt)_2$, LiBr, Et_3N, THF, 10–25 °C, 16–20 h; (b) for **59**, **60**, **62**, **63**: **29**, DBU, MeCN, 20–25 °C, 16–18 h; (c) for **61**, **64**: 4-bromo-1H-pyrazole, DBU, MeCN, 25 °C, 18 h; (d) B_2Pin_2, KOAc, XPhos Pd G3, 1,4-dioxane, 65 °C, 2 h.

With pyrazole boronates **31** and **59–64** in hand, the syntheses were completed as shown in **Scheme 5**. Suzuki - Miyaura coupling of either **47** or **52** with the pyrazole boronates **31** and **59–64** installed the pyrazine 4-substituent. In the case of coupling reactions with **52**, coupling mediated by Pd(*t*-$Bu_3P)_2$ at ambient temperature proceeded with very high regioselectivity for coupling at the desired pyrazolo[1,5-a]pyrazine 4-position. The regiochemical outcome of this Suzuki-Miyaura reaction sequence was established by the sequential Suzuki-Miyaura coupling of **52** with **62** (*cis* isomer) followed by Suzuki-Miyaura coupling with1-methyl-4-(4,4,5,5-tetramethyl-1,3,2-dioxaborolan-2-yl)-1H-pyrazole. This reaction sequence afforded a sample of **21** which was identical in all respects with the **21** prepared previously from compound **47**. Reversal of the order of Suzuki-Miyaura coupling steps (Suzuki-Miyaura coupling of **52** with 1-methyl-4-(4,4,5,5-tetramethyl-1,3,2-dioxaborolan-2-yl)-1H-pyrazole, followed by Suzuki-Miyaura coupling with **62**) afforded a product that was clearly distinguished from **21**. In the case of **67** and **68**, a second Suzuki-Miyaura coupling with the appropriate pyrazole boronate[53] mediated by palladium with X-Phos as supporting ligand installed the necessary substituents at the pyrazolo[1,5-a]pyrazine 6-position and was followed by deprotection (if required) to yield **23–28**. The azetidine analogs **11–16** were prepared by BOC deprotection of **65**, followed by appropriate functionalization of the azetidine NH of **66** by reductive amination (**12**, **13**), acylation (**14**), or alkylation (**11**, **15**, **16**).

Scheme 5: Synthesis of test compounds **11–28**

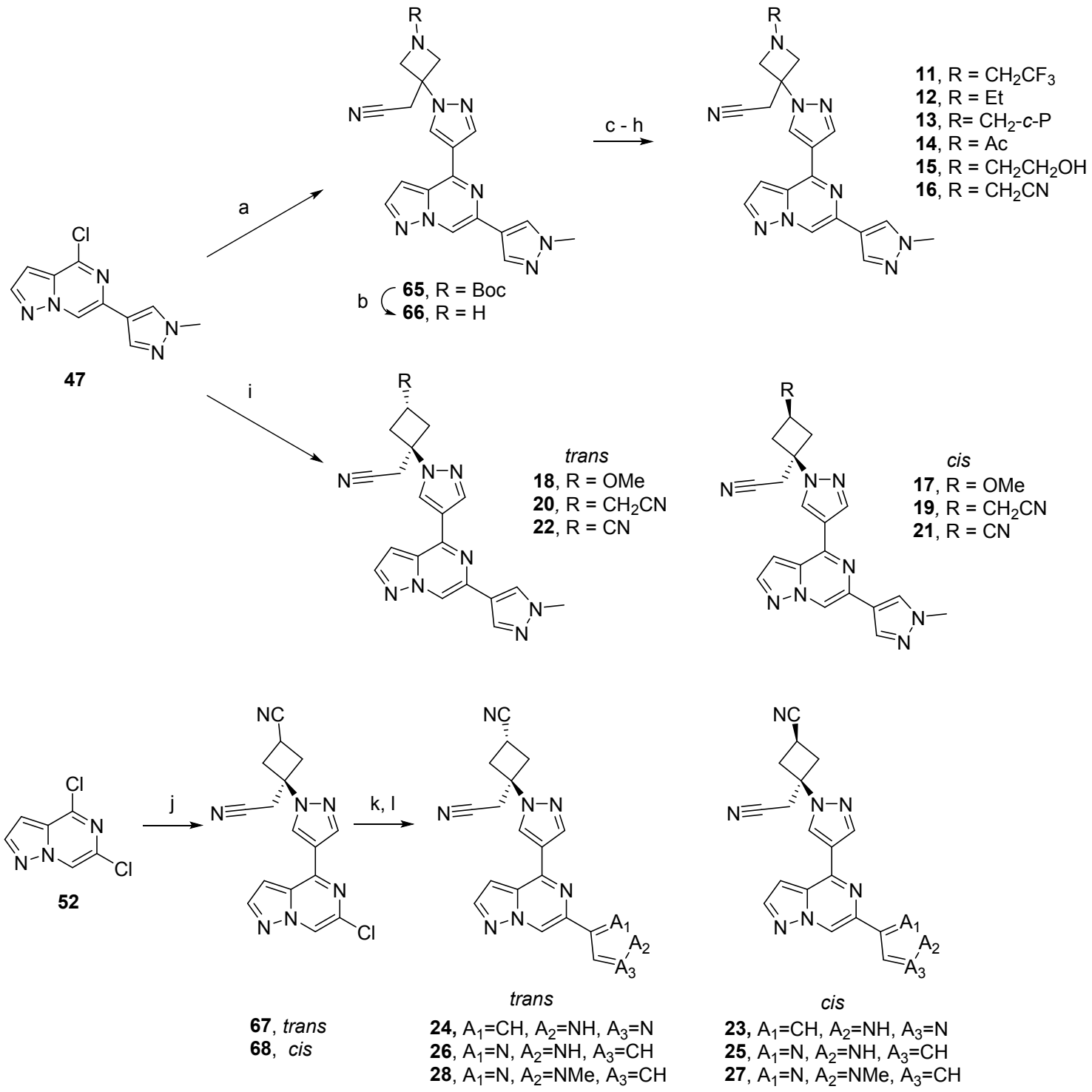

Reagents and conditions: (a) **31**, K_3PO_4, XPhos Pd G2, 1,4-dioxane, H_2O, 60 °C, 5 h; (b) (1) TFA, CH_2Cl_2, 20 °C, 90 min; (2) PS-carbonate; (c) CF_3CH_2OTf, DIEA, DMF, 20 °C, 18 h; (d) CH_3CHO, NaOAc, $NaBH(OAc)_3$, MeOH, 25 °C, 16 h; (e) *c*-PrCHO, NaOAc, $NaBH(OAc)_3$, MeOH, 25 °C, 16 h; (f) Ac_2O, Et_3N, CH_2Cl_2, 25 °C, 2

h; (g) $BrCH_2CH_2OH$, K_2CO_3, MeCN, 50 °C, 64 h; (h) $BrCH_2CN$, DIEA, DMF, 20 °C, 22 h; (i) **59–64**, K_3PO_4, XPhos Pd G3, 1,4-dioxane, H_2O, 40–55 °C, 1–18 h; (j) **59** or **62**, K_3PO_4, Pd(*t*-$Bu_3P)_2$, 1,4-dioxane, H_2O, 25 °C, 2 h; (k) pyrazole boronate[56], K_3PO_4, XPhos Pd G3, 1,4-dioxane, H_2O, 60 °C, 1 h; (l) TFA, TFAA, 25 °C, 0.5–2 h.

Conclusion

The discovery of a small molecular inhibitor of IL-12 and IL-23 with cellular and *in vivo* activity has been accomplished through the identification and optimization of a potent series of TYK2 inhibitors binding to the ATP site in the JH1 domain. Structure-based design and electrostatic modeling led to identification of a kinase hinge core that provided TYK2 potency and an encouraging preclinical *In vitro* selectivity profile against the other JAK-family members from the onset. Further optimization *via* design of cyclobutane analogs which engaged the P-loop to further increase TYK2 selectivity over JAK1 and JAK2 as well as balancing physicochemical properties secured high permeability and low metabolic clearance in the series. The balanced level of JAK2 selectivity was identified through screening in human whole blood assays, directly measuring cytokine signaling and uncovered the complex heterodimer partnership of JAK2 and TYK2. Balanced inhibition of TYK2 and JAK2 drove desired inhibition of IL-12 and IL-23 whilst maintaining EPO inhibition within program objectives. This effort led to the identification of compound **22** (PF-06826647) which has completed a Phase 1 clinical trial in healthy subjects and subjects with plaque psoriasis patients (NCT03210961) and is currently in Phase 2 studies in multiple inflammatory disease indications.

Experimental Section:

All activities involving laboratory animals were carried out in accordance with federal, state, local, and institutional guidelines governing the use of laboratory animals in research and were reviewed and approved by Pfizer (or other) Institutional Animal Care and Use Committee. Pfizer animal care facilities that supported this work are fully accredited by AAALAC International.

All biochemical assays for Human Janus kinase (JAK) activity have been previously reported.[21] The microfluidic assay monitored phosphorylation of a synthetic peptide by the recombinant human

kinase domain (JAK1, JAK2, JAK3, and TYK2). Reaction mixtures contained 1 mM ATP Utilizing mobility shift technology (PerkinElmer LabChip® EZ Reader).

Human blood samples were collected from healthy donors via vein puncture in accordance with Pfizer protocols (Protocol No. GOHW RDP-01) approved by the Shulman Institutional Review Board. Inhibition of cytokine-induced phosphorylation of STATs by JAK inhibitors in Human whole blood has been previously reported.[4]

Imiquimod-induced skin inflammation model in mutant strain of mouse designated as TYK2 Val980Ile was carried out as previously published.[43, 44] The TYK2 Val980Ile mice were orally administered PF-06826647 or vehicle, followed by topical application of imiquimod on the shaved ear to develop inflammation.

X-ray Crystallography

Protein production and purification on the JH1 domain of TYK2 and JAK2 as previously reported.[21, 43] See supporting information for further details.

Synthesis

Chemistry General Methods and Compound Characterization

Reagents and solvents were obtained from Aldrich and/or Alfa and were used without further purification. Solvents were commercial anhydrous grades and were used as received. All reactions were conducted with continuous magnetic stirring under an atmosphere of dry nitrogen unless otherwise specified. Chromatographic purifications were affected by medium pressure ("flash") chromatography on silica gel unless noted otherwise.

All new compounds were characterized by proton (^{1}H) NMR spectra using Bruker spectrometers and are reported in parts per million (ppm) relative to the residual resonances of the deuterated solvent. Carbon (^{13}C) and fluorine (^{19}F) NMR spectra were recorded similarly. All ^{13}C NMR and ^{19}F NMR spectra were proton decoupled. Melting points were obtained on a Thomas Hoover Mel-Temp capillary melting point apparatus and are uncorrected. Elemental Analyses were performed by Intertek, 291 Rte. 22 East, PO Box 470, Whitehouse, NJ 08888.

Low-resolution mass spectrometry analyses were conducted on Waters Acquity UPLC and SQ systems. Signal acquisition conditions included: Waters Acquity HSS T3 C18 2.1 50mm column at 60 °C with 0.1% formic acid in water (v/v) as the mobile phase A; 0.1% formic acid in CH_3CN (v/v) as the mobile phase B; 1.25 mL/min as the flow rate and ESCI (ESI+/-, APCI+/-), 100-2000m/z scan, 0.4 sec scan time, Centroid as the MS method. High-resolution mass spectrometry analyses were conducted on an Agilent 6220 TOF mass spectrometer in positive or negative electrospray mode. The system was calibrated to greater than 1 ppm accuracy across the mass range prior to analyses. The samples were separated using UPLC on an Agilent 1200 system prior to mass spectrometric analysis.

Purity of test compounds was assessed by elemental analysis for C, H, and N; or by reversed-phase HPLC with UV detection at 210 nm. Analytical reversed-phase HPLC was carried out on an Waters Acquity HSS T3 2.1 mm x 100 mm (1.8 µm) column at 45 °C eluting with 5% (v/v) CH_3CN in water containing 0.1% CH_3SO_3H (v/v) to 100% CH_3CN over 8.2 min; then holding at 100% CH_3CN for 0.5 min, then returning to 5% (v/v) CH_3CN in water containing 0.1% CH_3SO_3H (v/v) and hold for 1.5 min at a flow rate of 0.4 mL per min. Compounds **12 – 14** were analyzed using a BCUltimate Xbridge C18 3.0 x 50mm (3.0 µm) column at 40 °C eluting with 1% to 5% (v/v) CH_3CN in water containing 0.1% TFA (v/v) over 1 min; then from 5% (v/v) CH_3CN in water containing 0.1% TFA (v/v) to 100% CH_3CN containing 0.1% TFA (v/v) over 5 min; then holding at 100% CH_3CN containing 0.1% TFA (v/v) for 2 min, then returning to 1.0% (v/v) CH_3CN in water containing 0.1% TFA (v/v) and hold for 2 min at a flow rate of 1.2 mL per min. All tested compounds returned combustion analyses within 0.4% of theoretical values or demonstrated HPLC purity >95%, unless otherwise noted.

Diethyl 1-(2-(1-methyl-1H-pyrazol-4-yl)-2-oxoethyl)-1H-pyrazole-3,5-dicarboxylate (43): Two reactions were carried out in parallel as follows: A solution of **41** (500 g, 2.46 mol) and diethyl 1H-pyrazole-3,5-dicarboxylate (**42**, 580 g, 2.73 mol) in DMF (8 L) was treated with Cs_2CO_3 (1050 g, 3.23 mol). The mixtures were stirred at 20 °C for 18 h. The two reaction mixtures were then combined, diluted with water (10 L) and extracted with CH_2Cl_2 (3 x 10 L). The combined extracts were dried (Na_2SO_4), concentrated, and purified by chromatography to give **43** (1.53 kg, 93%). ^{1}H

NMR (400 MHz, $CDCl_3$) δ 7.93 (s, 1H), 7.93 (s, 1H), 7.43 (s, 1H), 5.83 (s, 2H), 4.42 (q, *J*=7.03 Hz, 2H), 4.28 (q, *J*=7.03 Hz, 2H), 3.96 (s, 3H), 1.40 (t, *J*=7.03 Hz, 3H), 1.32 (t, *J*=7.03 Hz, 3H). LC-MS: 335 (MH^+).

Ethyl 4-hydroxy-6-(1-methyl-1H-pyrazol-4-yl)pyrazolo[1,5-a]pyrazine-2-carboxylate (44): Three reactions were carried out in parallel as follows: To a solution of **43** (510 g, 1.52 mol) in ethanol (6 L) was added NH_4OAc (352 g, 4.57 mol). The reaction mixtures were heated at 130 °C in an autoclave for 24 h. The reaction mixtures were cooled to 50 °C, combined, and filtered. The precipitate was washed with EtOH and dried under vacuum to provide **44** (1090 g, 83%). ^{1}H NMR (400 MHz, DMSO) δ 11.70 (br. s., 1H), 8.30 (s, 1H), 8.20 (s, 1H), 8.04 (s, 1H), 7.37 (s, 1H), 4.33 (q, *J*=7.03 Hz, 2H), 1.32 (t, *J*=7.28 Hz, 3H). LC-MS: 310 (MNa^+).

6-(1-Methyl-1H-pyrazol-4-yl)-4-oxo-4,5-dihydropyrazolo[1,5-a]pyrazine-2-carboxylic acid (45): Two reactions were carried out in parallel as follows: A solution of **44** (545 g, 1.9 mol) in MeOH (10 L) was treated with 1.0 M NaOH (5.75 L) at 20 °C for 18 h. The mixtures were acidified with 12 M HCl, combined, and concentrated to remove most of the MeOH. The precipitate was filtered, washed with water and dried to give **45** (1040 g, 100%). ^{1}H NMR (400 MHz, DMSO) δ 13.20 (br. s., 1H), 11.65 (s, 1H), 8.30 (s, 1H), 8.15 (s, 1H), 8.05 (s, 1H), 7.32 (s, 1H). LC-MS: 260 (MH^+).

6-(1-Methyl-1H-pyrazol-4-yl)pyrazolo[1,5-a]pyrazin-4(5H)-one (46): Five reactions were carried out in parallel as follows: Sulfolane (800 mL) was heated to 280 °C, after which **45** (85 g, 0.328 mol) was added in portions. The five reaction mixtures were stirred at 280 °C for 2 h, cooled to 25 °C, and stirred for 18 h. The reaction mixtures were combined, and the mixture was purified by chromatography eluting with petroleum ether-EtOAc (10:1 to 0:1), followed by CH_2Cl_2-MeOH (10:1) to give **46** (490 g, 75%). ^{1}H NMR (400 MHz, DMSO) δ 11.44 (br. s., 1H), 8.27 (s, 1H), 8.09 (s, 1H), 8.03 (s, 1H), 7.88 (d, *J*=2.01 Hz, 1H), 6.99 (d, *J*=1.51 Hz, 1H), 3.87 (s, 3H). LC-MS: 216 (MH^+).

4-Chloro-6-(1-methyl-1H-pyrazol-4-yl)pyrazolo[1,5-a]pyrazine (47): Two reactions were carried out in parallel as follows: A suspension of **46** (307 g, 1.43 mol) in MeCN (7.5 L) was treated with $POCl_3$ (2006 g, 13 mol) at 25 °C, then heated at 85 °C for 48 h. The reaction mixtures were

combined and filtered. The precipitate was washed with EtOAc and dried under vacuum. The dried precipitate was purified by chromatography to afford a yellow solid which was dissolved in CH_2Cl_2 (15 L) and washed with 1 M aq. $NaHCO_3$ (5 L). The CH_2Cl_2 was concentrated to remove about 13 L of solvent and the residue was diluted with MTBE (2 L) and petroleum ether (2 L). The mixture was filtered, and the precipitate was dried to afford **47** (385 g, 58%). ^{1}H NMR (500 MHz, DMSO) δ = 9.15 (s, 1H), 8.22 (s, 1H), 8.16 (d, *J*=2.2 Hz, 1H), 8.00 (s, 1H), 6.96 (d, *J*=2.0 Hz, 1H), 3.88 (s, 3H). ^{13}C(^{1}H) NMR (126 MHz, DMSO) δ 142.5, 142.3, 136.3, 132.6, 132.2, 129.1, 118.3, 116.0, 99.8, 38.7. LC-MS: 234 (MH^+, ^{35}Cl isotope). HRMS (ESI/QTOF) m/z: $[M + H]^+$ Calcd for $C_{10}H_8ClN_5$ 234.054; Found 234.0538. Analysis: Calcd for $C_{10}H_8ClN_5$: C, 51.40; H, 3.45; N, 29.97; Cl, 15.17%. Found: C, 51.16; H, 3.35; N, 30.35; Cl, 15.20%.

3-(Cyanomethylene)cyclobutane-1-carbonitrile (56): A solution of 3-oxocyclobutane-1-carbonitrile[45] (**53**, 14.5 g, 152 mmol) in THF (250 mL) was added to a mixture of $(EtO)_2P(O)CH_2CN$ (31.1 g, 175 mmol), LiBr (19.9 g, 229 mmol) and Et_3N (30.9 g, 305 mmol) in THF (300 mL) at 25 °C. After 16 h, the mixture was filtered, and the filtrate was concentrated. The residue was purified by chromatography to afford **56** (16.01 g, 89%). ^{1}H NMR (400 MHz, CD_3CN) δ: 5.38 (s, 1 H), 3.30 - 3.43 (m, 2 H), 3.16 - 3.30 (m, 3 H). LC-MS: 119 (MH^+).

(1*s*,3*s*)-3-(cyanomethyl)-3-(4-(4,4,5,5-tetramethyl-1,3,2-dioxaborolan-2-yl)-1H-pyrazol-1-yl)cyclobutane-1-carbonitrile (*cis* isomer, 62) and (1*r*,3*r*)-3-(Cyanomethyl)-3-(4-(4,4,5,5-tetramethyl-1,3,2-dioxaborolan-2-yl)-1H-pyrazol-1-yl)cyclobutane-1-carbonitrile (*trans* isomer, 59): To a solution of **29** (1.3 kg, 6.67 mol) in MeCN (43 L) were added **56** (953 g, 8 mol) and DBU (3.06 kg, 20.1 mol) at 20 °C. Stirring was continued at 20 °C for 16 h. The mixture was poured into 1 M aqueous KH_2PO4 (10 L) and extracted with EtOAc (5 x 5 L). The combined EtOAc extracts were concentrated and the residue was purified by chromatography to afford **59** (*trans* isomer, 610 g, 30%) and **62** (*cis* isomer, 250 g, 12%).**59** (*trans* isomer): ^{1}H NMR (400 MHz, $CDCl_3$) δ: 7.90 (s, 1 H), 7.88 (s, 1 H), 3.21 - 3.28 (m, 3 H), 3.19 (s, 2 H), 2.86 - 2.94 (m, 2 H), 1.33 (s, 12 H). ^{13}C(^{1}H) NMR (101 MHz, CD_3OD) δ: 147.5, 136.5, 122.5, 117.1, 85.0, 61.9, 37.5, 30.5, 25.3, 25.2, 17.2. LC-MS: 313 (MH^+). Melting point 137 – 140 °C.**62** (*cis* isomer): ^{1}H NMR (400 MHz, $CDCl_3$) δ: 7.86 (s, 2 H), 3.24 - 3.31 (m, 1 H), 3.13 - 3.21 (m, 2 H), 3.07 (s, 2 H), 2.96 - 3.04 (m, 2 H), 1.34 (s,

12 H). $^{13}C(^{1}H)$ NMR (101 MHz, CD_3OD) δ: 147.4, 135.9, 121.9, 117.4, 85.0, 76.0, 60.1, 38.0, 28.4, 25.3, 16.2. LC-MS: 313 (MH^+). Melting point 95 – 98 °C.

(1*r*,3*r*)-3-(Cyanomethyl)-3-(4-(6-(1-methyl-1H-pyrazol-4-yl)pyrazolo[1,5-a]pyrazin-4-yl)-1H-pyrazol-1-yl)cyclobutane-1-carbonitrile (*trans* isomer, 22): To a solution of **59** (3.38 g, 10.8 mmol) and **47** (2.20 g, 9.4 mmol) in 1,4-dioxane (47.1 mL) was added 2 M aqueous K_3PO_4 (14.1 mL). Nitrogen was bubbled through the mixture for 5 min at 25 °C, after which XPhos Pd G2 (37.0 mg, 0.047 mmol) was added. The mixture was heated at 40 °C for 18 h, and then was heated to 80 °C to dissolve the precipitated product. The aqueous layer was removed while maintaining the temperature at 80 °C, then the warm 1,4-dioxane phase was added to EtOH (471 mL, previously preheated to 50 °C). The mixture was stirred for 10 min at 50 °C before being removed from heat. Stirring at 25 °C was continued for 6 h. The precipitated solid was filtered and washed with EtOH (2 x 25 mL), water (2 x 50 mL), and EtOH (2 x 25 mL). The precipitate was dried under vacuum to afford **22** (3.61 g, 74%). A sample of **22** (500 mg, 1.30 mmol) was heated in 1,4-dioxane (6.5 mL) at 80 °C until all of the material was dissolved. 1,2-Bis(diphenylphosphino)ethane (7.8 mg, 0.019 mmol) was added and heating at 80 °C was continued for 4 h, then the 1,4-dioxane phase was added to EtOH (58.7 mL, previously preheated to 50 °C). An additional 6.5 mL of preheated EtOH was used to rinse the reaction vessel. The mixture was removed from heat. Stirring at 25 °C was continued for 18 h. The solid was filtered and washed with EtOH (2 x 5 mL), water (5 mL), then EtOH (3 x 5 mL). The precipitate was dried under vacuum to afford **22** (450 mg, 90%). ^{1}H NMR (400 MHz, DMSO) δ: 9.02 (s, 1 H) 8.92 (s, 1 H) 8.52 (s, 1 H) 8.37 (s, 1 H) 8.19 (s, 1 H) 8.16 (s, 1 H) 7.45 (s, 1 H) 3.91 (s, 3 H) 3.55 - 3.65 (m, 1 H) 3.52 (s, 2 H) 3.22 - 3.38 (m, 2 H) 2.85 - 3.00 (m, 2 H). $^{13}C(^{1}H)$ NMR (126 MHz, DMSO) δ: 145.2, 142.5, 140.2, 137.1, 133.8, 131.4, 129.8, 129.5, 122.3, 121.1, 120.3, 117.3, 114.5, 99.9, 61.5, 39.3, 36.3, 29.7, 16.1. LC-MS: 384 (MH^+). HRMS (ESI/QTOF) m/z: $[M + H]^+$ Calcd for $C_{20}H_{17}N_9$ 384.1679; Found 384.1674. HPLC purity: 99.39%. Melting point 213 – 215 °C.

Author Information:

Corresponding Authors

Brian S. Gerstenberger - Pfizer Inc, Cambridge, Massachusetts 02139, United States

ORCID.org/0000-0002-6553-1975; Email:brian.gerstenberger@pfizer.com

Stephen W. Wright - Pfizer Inc, Groton, Connecticut 06340, United States

ORCID.org/0000-0002-9785-5077; Email: stephen.w.wright@pfizer.com

Authors

Catherine Ambler - Pfizer Inc, Groton, Connecticut 06340, United States

Eric P. Arnold - Pfizer Inc, Groton, Connecticut 06340, United States

Mary-Ellen Banker - Pfizer Inc, Groton, Connecticut 06340, United States

Matthew F. Brown - Pfizer Inc, Groton, Connecticut 06340, United States

James D. Clark - Pfizer Inc, Cambridge, Massachusetts 02139, United States

Alpay Dermenci - Pfizer Inc, Groton, Connecticut 06340, United States

Martin E. Dowty - Pfizer Inc, Cambridge, Massachusetts 02139, United States

Andrew Fensome - Pfizer Inc, Cambridge, Massachusetts 02139, United States

orcid.org/0000-0001-8916-1895

Susan Fish - Pfizer Inc, Cambridge, Massachusetts 02139, United States

Matthew M. Hayward - Pfizer Inc, Groton, Connecticut 06340, United States

Martin Hegen - Pfizer Inc, Cambridge, Massachusetts 02139, United States

Brett D. Hollingshead - Pfizer Inc, Cambridge, Massachusetts 02139, United States

John D. Knafels - Pfizer Inc, Groton, Connecticut 06340, United States

David W. Lin - Pfizer Inc, Groton, Connecticut 06340, United States

Tsung H. Lin - Pfizer Inc, Cambridge, Massachusetts 02139, United States

Dafydd R. Owen - Pfizer Inc, Cambridge, Massachusetts 02139, United States

Eddine Saiah - Pfizer Inc, Cambridge, Massachusetts 02139, United States

Raman Sharma - Pfizer Inc, Groton, Connecticut 06340, United States

Felix F. Vajdos - Pfizer Inc, Groton, Connecticut 06340, United States

Li Xing - Pfizer Inc, Cambridge, Massachusetts 02139, United States

ORCID.org/0000-0002-9056-7996

Xiaojing Yang - Pfizer Inc, Groton, Connecticut 06340, United States

Xin Yang - Pfizer Inc, Groton, Connecticut 06340, United States

Author Contributions

The manuscript was written through contributions of all authors. All authors have given approval to the final version of the manuscript.

Notes

The authors declare no competing financial interest.

Acknowledgments:

The authors thank Ms. Chao Li for assistance with determinations of purity by HPLC. The authors thank Chaoyan Li, Sheng Tan, Konghua Jing, Guagnyin Zhang, and Xuejyuan Li from WuXi AppTec for assistance with synthesis of compound **12-15**, **27**, and **28**.

Accession Codes

Atomic coordinates for the X-ray structure of compound **11** in TYK2 (PDB code 6X8F) and JAK2 (PDB code 6X8E) and compound **22** in TYK2 (PDB code 6X8G) are available from the RCSB Protein Data Bank (www.rcsb.org).

Abbreviations Used:

B_2Pin_2, bis(pinacolato)diboron; C_{av}, average concentration; CL_b, blood clearance; c-Pr, cyclopropyl; CYP450, cytochrome P450; DIEA, diisopropylethylamine; dppf, 1,1'-bis(diphenylphosphino)ferrocene; EPO, erythropoietin; GvHD, graft-versus-host disease; HHEP, human hepatocytes; HLM, human liver microsome; HS, hidradenitis suppurativa; HWB, human whole blood; IBD, inflammatory bowel disease; IC_{xx}, % average daily inhibition; IFN, Interferon; IL, Interleukin; JAK, Janus kinase; JAK1, Janus kinase 1; JAK2, Janus kinase 2; JAK3, Janus kinase 3; JH1, Janus homology 1; JH2, Janus homology 2; LipE, lipophilic efficiency; MDCK-LE, Madin-Darby canine kidney cell line low efflux permeability assay; nM, nanomolar; PBPK, physiologically based pharmacokinetics; P-loop, fingerprint ATP binding motif Gly-X-X-Gly-X-Gly-Lys-Thr/Ser; PS-carbonate, polystyrene supported (benzyltriethyl)ammonium carbonate; PsO, psoriasis; RA, rheumatoid arthritis; SDD, spray dried dispersion; sfLogD, shake-flask LogD; STAT, signal transducer and activator of transcription; TPO, thrombopoietin; TYK2, tyrosine kinase 2; UC, ulcerative colitis; V_{ss}, steady state volume of distribution;

Ancillary Information:

The Supporting Information is available free of charge on the ACS Publications website at DOI: <TBD>

- 1) Synthesis of **8 – 10**, **17 – 20**, and **23 – 28**; 2) Kinase profiling for compound **22** at 1 uM**;** 3) X-ray crystallography methods; 4) Copies of ^{1}H and ^{13}C NMR spectra and HPLC traces of compounds **8 – 28**. (PDF)
- Molecular formula strings (CSV)

References:

1. Gadina, M.; Gazaniga, N.; Vian, L.; Furumoto, Y. Small molecules to the rescue: Inhibition of cytokine signaling in immune-mediated diseases. *Journal of Autoimmunity* **2017,** 85, 20-31, DOI: 10.1016/j.jaut.2017.06.006

2. Schwartz, D. M.; Kanno, Y.; Villarino, A.; Ward, M.; Gadina, M.; O'Shea, J. J. JAK inhibition as a therapeutic strategy for immune and inflammatory diseases. *Nature Reviews Drug Discovery* **2017,** 16, 843, DOI: 10.1038/nrd.2017.201

3. Solimani, F.; Meier, K.; Ghoreschi, K. Emerging topical and systemic JAK inhibitors in dermatology. *Frontiers in Immunology* **2019,** 10, 2847, DOI: 10.3389/fimmu.2019.02847

4. Dowty, M. E.; Lin, T. H.; Jesson, M. I.; Hegen, M.; Martin, D. A.; Katkade, V.; Menon, S.; Telliez, J.-B. Janus kinase inhibitors for the treatment of rheumatoid arthritis demonstrate similar profiles of in vitro cytokine receptor inhibition. *Pharmacol Res Perspect* **2019,** 7, e00537, DOI: 10.1002/prp2.537

5. Villarino, A. V.; Kanno, Y.; Ferdinand, J. R.; O'Shea, J. J. Mechanisms of Jak/STAT signaling in immunity and disease. *The Journal of Immunology* **2015,** 194, 21-27, DOI: 10.4049/jimmunol.1401867

6. Sohn, S. J.; Barrett, K.; Van Abbema, A.; Chang, C.; Kohli, P. B.; Kanda, H.; Smith, J.; Lai, Y.; Zhou, A.; Zhang, B.; Yang, W.; Williams, K.; Macleod, C.; Hurley, C. A.; Kulagowski, J. J.; Lewin-Koh, N.; Dengler, H. S.; Johnson, A. R.; Ghilardi, N.; Zak, M.; Liang, J.; Blair, W. S.; Magnuson, S.; Wu, L. C. A restricted role for TYK2 catalytic activity in human cytokine responses revealed by novel TYK2-selective inhibitors. *J Immunol* **2013,** 191, 2205-2216, DIO: 10.4049/jimmunol.1202859

7. Dendrou, C. A.; Cortes, A.; Shipman, L.; Evans, H. G.; Attfield, K. E.; Jostins, L.; Barber, T.; Kaur, G.; Kuttikkatte, S. B.; Leach, O. A.; Desel, C.; Faergeman, S. L.; Cheeseman, J.; Neville, M. J.; Sawcer, S.; Compston, A.; Johnson, A. R.; Everett, C.; Bell, J. I.; Karpe, F.; Ultsch, M.; Eigenbrot, C.; McVean, G.; Fugger, L. Resolving TYK2 locus genotype-to-phenotype differences

in autoimmunity. *Science Translational Medicine* **2016,** 8, 363ra149, DOI: 10.1126/scitranslmed.aag1974

8. Gorman, J. A.; Hundhausen, C.; Kinsman, M.; Arkatkar, T.; Allenspach, E. J.; Clough, C.; West, S. E.; Thomas, K.; Eken, A.; Khim, S.; Hale, M.; Oukka, M.; Jackson, S. W.; Cerosaletti, K.; Buckner, J. H.; Rawlings, D. J. The TYK2-P1104A autoimmune protective variant limits coordinate signals required to generate specialized T cell subsets. *Frontiers in Immunology* **2019,** 10, 44, DOI: 10.3389/fimmu.2019.00044

9. Zaghi, D.; Krueger, G. G.; Callis, K. D. Ustekinumab: a review in the treatment of plaque psoriasis and psoriatic arthritis. *Journal of Drugs in Dermatology: JDD* **2012,** 11, 160-167

10. Lamb, Y. N.; Duggan, S. T. Ustekinumab: A review in moderate to severe Crohn's disease. *Drugs* **2017,** 77, 1105-1114, DOI: 10.1007/s40265-017-0765-6

11. Sands, B. E.; Sandborn, W. J.; Panaccione, R.; O'Brien, C. D.; Zhang, H.; Johanns, J.; Adedokun, O. J.; Li, K.; Peyrin-Biroulet, L.; Van Assche, G. Ustekinumab as induction and maintenance therapy for ulcerative colitis. *New England Journal of Medicine* **2019,** 381, 1201-1214

12. Yang, E. J.; Smith, M. P.; Ly, K.; Bhutani, T. Evaluating guselkumab: an anti-IL-23 antibody for the treatment of plaque psoriasis. *Drug Des Devel Ther* **2019,** 13, 1993-2000, DOI: 10.2147/DDDT.S137588

13. Papp, K. A.; Blauvelt, A.; Bukhalo, M.; Gooderham, M.; Krueger, J. G.; Lacour, J.-P.; Menter, A.; Philipp, S.; Sofen, H.; Tyring, S.; Berner, B. R.; Visvanathan, S.; Pamulapati, C.; Bennett, N.; Flack, M.; Scholl, P.; Padula, S. J. Risankizumab versus Ustekinumab for moderate-

to-severe plaque psoriasis. *New England Journal of Medicine* **2017,** 376, 1551-1560, DOI: 10.1056/NEJMoa1607017

14. He, X.; Chen, X.; Zhang, H.; Xie, T.; Ye, X.-Y. Selective Tyk2 inhibitors as potential therapeutic agents: a patent review (2015–2018). *Expert Opinion on Therapeutic Patents* **2019,** 29, 137-149, DOI: 10.1080/13543776.2019.1567713

15. Papp, K.; Gordon, K.; Thaçi, D.; Morita, A.; Gooderham, M.; Foley, P.; Girgis, I. G.; Kundu, S.; Banerjee, S. Phase 2 trial of selective tyrosine kinase 2 inhibition in psoriasis. *New England Journal of Medicine* **2018,** 379, 1313-1321, DOI: 10.1056/NEJMoa1806382

16. Burke, J. R.; Cheng, L.; Gillooly, K. M.; Strnad, J.; Zupa-Fernandez, A.; Catlett, I. M.; Zhang, Y.; Heimrich, E. M.; McIntyre, K. W.; Cunningham, M. D.; Carman, J. A.; Zhou, X.; Banas, D.; Chaudhry, C.; Li, S.; D'Arienzo, C.; Chimalakonda, A.; Yang, X.; Xie, J. H.; Pang, J.; Zhao, Q.; Rose, S. M.; Huang, J.; Moslin, R. M.; Wrobleski, S. T.; Weinstein, D. S.; Salter-Cid, L. M. Autoimmune pathways in mice and humans are blocked by pharmacological stabilization of the TYK2 pseudokinase domain. *Science Translational Medicine* **2019,** 11, eaaw1736, DOI: 10.1126/scitranslmed.aaw1736

17. O'Shea, J. J.; Gadina, M. Selective Janus kinase inhibitors come of age. *Nature Reviews Rheumatology* **2019,** 15, 74-75, DOI: 10.1038/s41584-018-0155-9

18. Hosseini, A.; Gharibi, T.; Marofi, F.; Javadian, M.; Babaloo, Z.; Baradaran, B. Janus kinase inhibitors: A therapeutic strategy for cancer and autoimmune diseases. *Journal of Cellular Physiology* **2020**, 235(9):5903-5924, DOI: 10.1002/jcp.29593

19. Wrobleski, S. T.; Moslin, R.; Lin, S.; Zhang, Y.; Spergel, S.; Kempson, J.; Tokarski, J. S.; Strnad, J.; Zupa-Fernandez, A.; Cheng, L.; Shuster, D.; Gillooly, K.; Yang, X.; Heimrich, E.;

McIntyre, K. W.; Chaudhry, C.; Khan, J.; Ruzanov, M.; Tredup, J.; Mulligan, D.; Xie, D.; Sun, H.; Huang, C.; D'Arienzo, C.; Aranibar, N.; Chiney, M.; Chimalakonda, A.; Pitts, W. J.; Lombardo, L.; Carter, P. H.; Burke, J. R.; Weinstein, D. S. Highly selective inhibition of tyrosine kinase 2 (TYK2) for the treatment of autoimmune siseases: Discovery of the allosteric inhibitor BMS-986165. *Journal of Medicinal Chemistry* **2019,** 62, 8973-8995, DOI: 10.1021/acs.jmedchem.9b00444

20. An Investigational Study to Evaluate Experimental Medication BMS-986165 Compared to Placebo and a Currently Available Treatment in Participants With Moderate-to-Severe Plaque Psoriasis. ClinicalTrials.gov; U.S. National Institutes of Health: Bethesda, MD, 2020; NCT03611751, https://clinicaltrials.gov/ct2/show/NCT03611751 (accessed August 2, 2018)

21. Fensome, A.; Ambler, C. M.; Arnold, E.; Banker, M. E.; Brown, M. F.; Chrencik, J.; Clark, J. D.; Dowty, M. E.; Efremov, I. V.; Flick, A.; Gerstenberger, B. S.; Gopalsamy, A.; Hayward, M. M.; Hegen, M.; Hollingshead, B. D.; Jussif, J.; Knafels, J. D.; Limburg, D. C.; Lin, D.; Lin, T. H.; Pierce, B. S.; Saiah, E.; Sharma, R.; Symanowicz, P. T.; Telliez, J.-B.; Trujillo, J. I.; Vajdos, F. F.; Vincent, F.; Wan, Z.-K.; Xing, L.; Yang, X.; Yang, X.; Zhang, L. Dual inhibition of TYK2 and JAK1 for the treatment of autoimmune diseases: Discovery of ((S)-2,2-Difluorocyclopropyl)((1R,5S)-3-(2-((1-methyl-1H-pyrazol-4-yl)amino)pyrimidin-4-yl)-3,8-diazabicyclo[3.2.1]octan-8-yl)methanone (PF-06700841). *Journal of Medicinal Chemistry* **2018,** 61, 8597-8612, DOI: 10.1021/acs.jmedchem.8b00917

22. Banfield, C.; Scaramozza, M.; Zhang, W.; Kieras, E.; Page, K. M.; Fensome, A.; Vincent, M.; Dowty, M. E.; Goteti, K.; Winkle, P. J.; Peeva, E. The safety, tolerability, pharmacokinetics, and pharmacodynamics of a TYK2/JAK1 inhibitor (PF-06700841) in healthy subjects and patients

with plaque psoriasis. *The Journal of Clinical Pharmacology* **2018,** 58, 434-447, DOI: 10.1002/jcph.1046

23. Vainchenker, W.; Favale, F. Myelofibrosis, JAK2 inhibitors and erythropoiesis. *Leukemia* **2013,** 27, 1219-1223, DOI: 10.1038/leu.2013.72

24. A Study to Evaluate Safety and Efficacy of PF-06826647 For Moderate To Severe Plaque Psoriasis. ClinicalTrials.gov; U.S. National Institutes of Health: Bethesda, MD, 2018; NCT03895372, https://clinicaltrials.gov/ct2/show/NCT03895372 (accessed March 29, 2019)

25. A Study To Evaluate The Safety And Efficacy Of PF-06826647 In Participants With Moderate To Severe Ulcerative Colitis. ClinicalTrials.gov; U.S. National Institutes of Health: Bethesda, MD, 2020; NCT04209556, https://clinicaltrials.gov/ct2/show/NCT04209556 (accessed December 24, 2019)

26. A Study to Evaluate the Safety and Efficacy of PF-06650833, PF-06700841, and PF 06826647 in Adults With Hidradenitis Suppurativa. ClinicalTrials.gov; U.S. National Institutes of Health: Bethesda, MD, 2020; NCT04092452, https://clinicaltrials.gov/ct2/show/NCT04092452 (accessed September 17, 2019)

27. Fensome, A.; Ambler, C. M.; Arnold, E.; Banker, M. E.; Clark, J. D.; Dowty, M. E.; Efremov, I. V.; Flick, A.; Gerstenberger, B. S.; Gifford, R. S.; Gopalsamy, A.; Hegen, M.; Jussif, J.; Limburg, D. C.; Lin, T. H.; Pierce, B. S.; Sharma, R.; Trujillo, J. I.; Vajdos, F. F.; Vincent, F.; Wan, Z.-K.; Xing, L.; Yang, X.; Yang, X. Design and optimization of a series of 4-(3-azabicyclo[3.1.0]hexan-3-yl)pyrimidin-2-amines: Dual inhibitors of TYK2 and JAK1. *Bioorganic & Medicinal Chemistry* **2020**, 115481-115491, DOI: 10.1016/j.bmc.2020.115481

28. Dowty, M. E.; Lin, T. H.; Jesson, M. I.; Hegen, M.; Martin, D. A.; Katkade, V.; Menon, S.; Telliez, J.-B. Janus kinase inhibitors for the treatment of rheumatoid arthritis demonstrate similar profiles of in vitro cytokine receptor inhibition. *Pharmacol Res Perspect* **2019,** 7, e00537-e00537, DOI: 10.1002/prp2.537

29. Clark, J. D.; Flanagan, M. E.; Telliez, J.-B. Discovery and development of Janus kinase (JAK) inhibitors for inflammatory diseases. *Journal of Medicinal Chemistry* **2014,** 57, 5023-5038, DOI: 10.1021/jm401490p

30. Xing, L.; Klug-Mcleod, J.; Rai, B.; Lunney, E. A. Kinase hinge binding scaffolds and their hydrogen bond patterns. *Bioorganic & Medicinal Chemistry* **2015,** 23, 6520-6527, DOI: 10.1016/j.bmc.2015.08.006

31. Mohan, N.; Suresh, C. H. A molecular electrostatic potential analysis of hydrogen, halogen, and dihydrogen bonds. *The Journal of Physical Chemistry A* **2014,** 118, 1697-1705, DOI: 10.1021/jp4115699

32. Qiao, L.; Choi, S.; Case, A.; Gainer, T. G.; Seyb, K.; Glicksman, M. A.; Lo, D. C.; Stein, R. L.; Cuny, G. D. Structure-activity relationship study of EphB3 receptor tyrosine kinase inhibitors. *Bioorg. Med. Chem. Lett.* **2009,** 19, 6122-6126, DOI: 10.1016/j.bmcl.2009.09.010

33. Ninkovic, S.; Braganza, J. F.; Collins, M. R.; Kath, J. C.; Li, H.; Richter, D. T. Preparation of Heterocyclylaminopyrazine Derivatives for Use as CHK-1 Inhibitors. WO2010016005A1, 2010.

34. Bach Tana, J.; Perez Crespo, D.; Llera Soldevila, O.; Esteve Trias, C.; Taboada Martinez, L. Preparation of 2-(Pyrazolo[1,5-a]pyrazin-3-yl)pyrimidine and 2-(Pyrazolo[1,5-a]pyridin-3-yl)pyrimidine Derivatives as JAK Inhibitors for Therapy. WO2015086693A1, 2015.

35. Currie, K. S.; Du, Z.; Farand, J.; Guerrero, J. A.; Katana, A. A.; Kato, D.; Lazerwith, S. E.; Li, J.; Link, J. O.; Mai, N.; Notte, G.; Pyun, H.-J.; Sangi, M.; Schmitt, A. C.; Schrier, A. J.; Stevens, K. L.; Venkataramani, C.; Watkins, W. J.; Yang, Z.-Y.; Zablocki, J.; Zipfel, S. Azabicyclyloxyalkylpyrrolidinone Derivatives as Syk Inhibitors and Their Preparation. WO2015017610A1, 2015.

36. Allen, S.; Boys, M. L.; Chicarelli, M. J.; Fell, J. B.; Fischer, J. P.; Gaudino, J.; Hicken, E. J.; Hinklin, R. J.; Kraser, C. F.; Laird, E.; Robinson, J. E.; Tang, T. P.; Burgess, L. E.; Rieger, R. A.; Pheneger, J.; Satoh, Y.; Leftheris, K.; Raheja, R. K.; Bennett, B. L. 4,6-Disubstituted-pyrazolo[1,5-a]pyrazines as Janus Kinase Inhibitors and Their Preparation. WO2016090285A1, 2016.

37. Andrews, S. W.; Blake, J. F.; Haas, J.; Jiang, Y.; Kolakowski, G. R.; Moreno, D. A.; Ren, L.; Walls, S. M. Preparation of Substituted Pyrazolo[1,5-a]pyrazine Compounds as RET Kinase Inhibitors. WO2018136661A1, 2018.

38. Fradera, X.; Methot, J. L.; Achab, A.; Christopher, M.; Altman, M. D.; Zhou, H.; McGowan, M. A.; Kattar, S. D.; Wilson, K.; Garcia, Y.; Augustin, M. A.; Lesburg, C. A.; Shah, S.; Goldenblatt, P.; Katz, J. D. Design of selective PI3Kδ inhibitors using an iterative scaffold-hopping workflow. *Bioorg. Med. Chem. Lett.* **2019,** 29, 2575-2580, DOI: 10.1016/j.bmcl.2019.08.004

39. Chrencik, J. E.; Patny, A.; Leung, I. K.; Korniski, B.; Emmons, T. L.; Hall, T.; Weinberg, R. A.; Gormley, J. A.; Williams, J. M.; Day, J. E.; Hirsch, J. L.; Kiefer, J. R.; Leone, J. W.; Fischer, H. D.; Sommers, C. D.; Huang, H.-C.; Jacobsen, E. J.; Tenbrink, R. E.; Tomasselli, A. G.; Benson, T. E. Structural and Thermodynamic Characterization of the TYK2 and JAK3 Kinase Domains in

Complex with CP-690550 and CMP-6. *Journal of Molecular Biology* **2010,** 400, 413-433, DOI: 10.1016/j.jmb.2010.05.020

40. Varma, M. V.; Steyn, S. J.; Allerton, C.; El-Kattan, A. F. Predicting clearance mechanism in drug discovery: Extended Clearance Classification System (ECCS). *Pharm Res* **2015,** 32, 3785-3802, DOI: 10.1007/s11095-015-1749-4

41. Dowty, M. E.; Hu, G.; Hua, F.; Shilliday, F. B.; Dowty, H. V. Drug design structural alert: Formation of trifluoroacetaldehyde through N-dealkylation is linked to testicular lesions in rat. *International Journal of Toxicology* **2011,** 30, 546-550, DOI: 10.1177/1091581811413833

42. Di, L.; Whitney-Pickett, C.; Umland, J. P.; Zhang, H.; Zhang, X.; Gebhard, D. F.; Lai, Y.; Federico, J. J.; Davidson, R. E.; Smith, R.; Reyner, E. L.; Lee, C.; Feng, B.; Rotter, C.; Varma, M. V.; Kempshall, S.; Fenner, K.; El-kattan, A. F.; Liston, T. E.; Troutman, M. D. Development of a new permeability assay using low-efflux MDCKII cells. *Journal of Pharmaceutical Sciences* **2011,** 100, 4974-4985, DOI: 10.1002/jps.22674

43. Vazquez, M. L.; Kaila, N.; Strohbach, J. W.; Trzupek, J. D.; Brown, M. F.; Flanagan, M. E.; Mitton-Fry, M. J.; Johnson, T. A.; TenBrink, R. E.; Arnold, E. P.; Basak, A.; Heasley, S. E.; Kwon, S.; Langille, J.; Parikh, M. D.; Griffin, S. H.; Casavant, J. M.; Duclos, B. A.; Fenwick, A. E.; Harris, T. M.; Han, S.; Caspers, N.; Dowty, M. E.; Yang, X.; Banker, M. E.; Hegen, M.; Symanowicz, P. T.; Li, L.; Wang, L.; Lin, T. H.; Jussif, J.; Clark, J. D.; Telliez, J.-B.; Robinson, R. P.; Unwalla, R. Identification of N-{cis-3-[Methyl(7H-pyrrolo[2,3-d]pyrimidin-4-yl)amino]cyclobutyl}propane-1-sulfonamide (PF-04965842): A selective JAK1 clinical candidate for the treatment of autoimmune diseases. *Journal of Medicinal Chemistry* **2018,** 61, 1130-1152, DOI: 10.1021/acs.jmedchem.7b01598

44. Bucher, D.; Stouten, P.; Triballeau, N. Shedding light on important waters for drug design: Simulations versus grid-based methods. *Journal of Chemical Information and Modeling* **2018,** 58, 692-699, DOI: 10.1021/acs.jcim.7b00642

45. Card, A.; Caldwell, C.; Min, H.; Lokchander, B.; Hualin, X.; Sciabola, S.; Kamath, A. V.; Clugston, S. L.; Tschantz, W. R.; Leyu, W.; Moshinsky, D. J. High-throughput biochemical kinase selectivity assays: Panel development and screening applications. *Journal of Biomolecular Screening* **2008,** 14, 31-42, DOI: 10.1177/1087057108326663

46. Feng, B.; West, M.; Patel, N. C.; Wager, T.; Hou, X.; Johnson, J.; Tremaine, L.; Liras, J. Validation of human MDR1-MDCK and BCRP-MDCK cell lines to improve the prediction of brain penetration. *Journal of Pharmaceutical Sciences* **2019,** 108, 2476-2483, DOI: 10.1016/j.xphs.2019.02.005

47. Obach, R. S. Predicting clearance in humans from In Vitro data. *Current Topics in Medicinal Chemistry* **2011,** 11, 334-339, DOI: 10.2174/156802611794480873

48. Hosea, N. A.; Collard, W. T.; Cole, S.; Maurer, T. S.; Fang, R. X.; Jones, H.; Kakar, S. M.; Nakai, Y.; Smith, B. J.; Webster, R.; Beaumont, K. Prediction of human pharmacokinetics from preclinical information: Comparative accuracy of quantitative prediction approaches. *The Journal of Clinical Pharmacology* **2009,** 49, 513-533, DOI: 10.1177/0091270009333209

49. Hak, L.; Katherine, M.; Masek, H.; Susan, F.; Lee, N.; Eva, N.; Martin, H.; James, D. Attenuating Janus kinases (JAK) by tofacitinib effectively prevented psoriasis pathology in various mouse skin inflammation models. *J Clin Cell Immunol* **2013,** 4, DOI: 10.4172/2155-9899.1000176

50. Gerstenberger, B. S.; Banker, M. E.; Clark, J. D.; Dowty, M. E.; Fensome, A.; Gifford, R.; Griffor, M. C.; Hegen, M.; Hollingshead, B. D.; Knafels, J. D.; Lin, T. H.; Smith, J. F.; Vajdos, F. F. Demonstration of In Vitro to In Vivo translation of a TYK2 inhibitor that shows cross species potency differences. *Scientific Reports* **2020,** 10, 8974, DOI: 10.1038/s41598-020-65762-y

51. Xu, J.; Cai, J.; Chen, J.; Zong, X.; Wu, X.; Ji, M.; Wang, P. An efficient synthesis of Baricitinib. *Journal of Chemical Research* **2016,** 40, 205-208, DOI: 10.3184/174751916X14569294811333

52. Taydakov, I. V.; Krasnoselskiy, S. S. Direct electrophilic acylation of n-substituted pyrazoles by anhydrides of carboxylic acids. *Synthesis* **2013,** 45, 2188-2192

53. Wright, S. W.; Arnold, E. P.; Yang, X. Steric redirection of alkylation in 1H-pyrazole-3-carboxylate esters. *Tetrahedron Letters* **2018,** 59, 402-405, DOI: 10.1016/j.tetlet.2017.12.052

54. Aicart, M.; Mavoungou-Gomès, L. Conversion des furfurylalkyl et arylcetones en derives de l'isocoumarine et de l'isoquinoleine. *Journal of Heterocyclic Chemistry* **1985,** 22, 921-925, DOI: 10.1002/jhet.5570220361

55. Rathke, M. W.; Nowak, M. The Horner-Wadsworth-Emmons modification of the Wittig reaction using triethylamine and lithium or magnesium salts. *The Journal of Organic Chemistry* **1985,** 50, 2624-2626, DOI: 10.1021/jo00215a004

56. For 23 and 24, Suzuki - Miyaura coupling was performed with tert-butyl 4-(4,4,5,5-tetramethyl-1,3,2-dioxaborolan-2-yl)-1H-pyrazole-1-carboxylate. For 25 and 26, Suzuki - Miyaura coupling was performed with 1-(tetrahydropyran-2-yl)-5-(4,4,5,5-tetramethyl-1,3,2-dioxaborolan-2-yl)pyrazole. For 27 and 28, Suzuki - Miyaura coupling was performed with 1-methyl-3-(4,4,5,5-tetramethyl-1,3,2-dioxaborolan-2-yl)-1H-pyrazole.

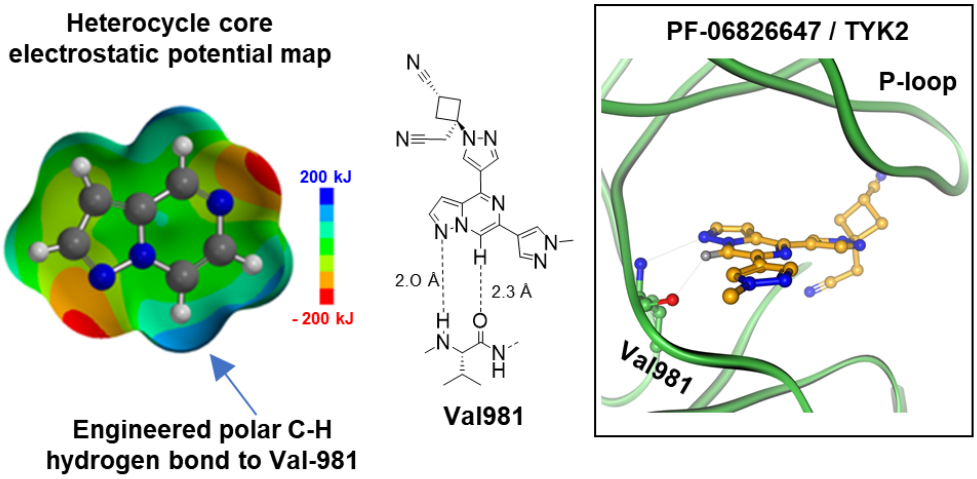

82x44mm (300 x 300 DPI)